International
Progress Report

IPR-06-17

Äspö Hard Rock Laboratory

Äspö Task Force on modelling of groundwater flow and transport of solutes

Modelling of Task 6D, 6E, 6F and 6F2 using the Posiva streamtube approach

Antti Poteri

VTT

August 2006

Svensk Kärnbränslehantering AB
Swedish Nuclear Fuel
and Waste Management Co
Box 5864
SE-102 40 Stockholm Sweden
Tel 08-459 84 00
+46 8 459 84 00
Fax 08-661 57 19
+46 8 661 57 19

Äspö Hard Rock Laboratory

Report no.
IPR-06-17
No.
F65K
Author
Antti Poteri
Date
August 2006
Checked by
Aimo Hautojärvi
Date
2006-11-03
Approved
Anders Sjöland
Date
2006-11-29

Äspö Hard Rock Laboratory

Äspö Task Force on modelling of groundwater flow and transport of solutes

Modelling of Task 6D, 6E, 6F and 6F2 using the Posiva streamtube approach

Antti Poteri

VTT

August 2006

Keywords: Fractured rock, Transport of solutes, Performance assessment, Site characterisation

Abstract

Task 6 studies solute transport through fractured rock both in the site characterisation and performance assessment conditions and especially the simplification made in the performance assessment models compared to the site characterisation models. The framework of the Task 6 modelling is a semi-synthetic model of the hydraulic features and microstructural model of the immobile pore space in the Task 6 modelling volume.

Modelling of the Tasks 6D, 6E, 6F and 6F2 presented in this report employs directly the semi-synthetic DFN and microstructural models of the Task 6C. This means that the geometry of the structures and the microstructural model are taken into account as they are defined in the Task 6C model or in the task definition.

Modelling indicates that it is very difficult to extrapolate performance assessment scale transport properties from the transport properties of the site characterisation scale. Solute transport in the site characterisation scale is governed by the microstructural model along the expected transport paths. In the performance assessment scale the averaging of the immobile zone transport properties extends much deeper in the rock matrix than in the site characterisation flow conditions. This may result a significant contrast between the retention properties that are observed in the site characterisation and in the performance assessment, because the governing retention zones can be totally different.

Modelling suggests that it is better to link the site characterisation and performance assessment models in the level of the retention processes than in the level of the retention parameters. Tracer experiments in the site characterisation conditions and the related modelling can be used to build confidence that the retention processes involved in the performance assessment models are appropriate for the fractured rock.

Sammanfattning

Task 6 studerar transport av lösta ämnen genom sprickigt berg under förhållanden som gäller inom platskaraktärisering och/eller inom säkerhetsanalys och särskilt de förenklingar som görs i säkerhetsanalysmodeller jämfört med platskaraktäriserings-modeller. Stommen för modelleringen inom Task 6 är en semi-syntetisk modell av hydrauliska enheter och en mikrostrukturmodell av det immobila porutrymmet i modellvolymen för Task 6.

Modelleringen av Tasks 6D, 6E, 6F och 6F2 som presenteras i den här rapporten utnyttjar direkt den semi-syntetiska DFN och mikrostrukturmodellerna från Task 6C. Det innebär att hänsyn tas till geometri på strukturer och mikrostrukturmodell på det sätt some definieras i modellen för Task 6C eller i uppgiftsdefinitionen.

Modelleringen indikerar att det är väldigt svårt att extrapolera transportegenskaper från säkerhetsanalysskala till platskaraktäriseringsskala. I platskaraktäriseringsskala styrs transporten av mikrostrukturmodellen längs den förväntade transportvägen. I säkerhetsanalysskala sträcker sig de medelvärdesbildade transportegenskaperna för stagnanta zoner mycket djupare in i bergmatrisen än vid flödesförhållanden enligt platskaraktäriseringen. Detta kan vara orsaken till de signifikanta skillnader i retentionsegenskaper som observeras i platskaraktärisering och säkerhetsanalys, eftersom den dominerande retentionszonen kan bli helt olika.

Modelleringen tyder på att det är bättre att länka platskarakteriseringsmodeller och säkerhetsanalysmodeller på nivån för retentionsprocesser istället för på nivån för retentionsparametrar. Transportexperiment och modellering av platskaraktäriserings-förhållanden kan användas för att ge förtroende för att de retentionsprocesser som ingår i säkerhetsanalysmodellerna är lämpliga för sprickigt berg.

Executive summary

Objective of the Task 6 is to bridge between the site characterisation and performance assessment models and to study the significance of the simplifications made in the performance assessment models. Task 6 is organised to a number of sub-tasks that concentrates on the specific aspects of the transport through fractured rock. Task 6D and Task 6E examine solute transport through a semi-synthetic fracture network in site characterisation and performance assessment flow conditions, respectively. Task 6F is a benchmark subtask that investigates transport through different types of fractures, and finally, Task 6F2 is a compilation of the different sensitivity analysis.

Modelling of the Task 6 is based on the approach where the flow and transport calculations are performed separately. Assessment of the tracer transport is performed separately from the groundwater flow calculations by employing transport properties of the particle pathways that are identified and quantified in the flow calculations.

The flow field is solved using a FEM based flow model FEFTRA. The flow solution is used for assessment of the flow paths and calculation of the transport properties along the flow paths. Flow paths are represented by the tracked particle pathways through the flow field. Important transport characteristics of the transport pathways are the hydrodynamic control of retention, i.e. the F-factor (or similar parameters β or WL/Q), and the advective delay along the flow paths that is also presented as the water residence time distribution.

The simplified flow conditions defined for the Task 6F and Task 6F2 enables assessment of the transport characteristics along the flow paths to be based directly on the task definitions. This approach has been applied in the modelling so that the F-factor and advective delay along the flow paths in Task 6F and Task 6F2 are based directly on the task definitions. Modelling of these tasks comprised only the transport modelling.

In all tasks the transport modelling is based on a semi-analytical approach. Transport and retention processes that are taken into account are advection, matrix diffusion and sorption. The modelling approach describes the layered structure of the immobile zones by a series of limited thickness immobile zones. This is equivalent with the layered structure as given in the microstructural model if the equivalent retention properties of the immobile zones are stronger for the layer that is closer to the fracture. This is the case in the Task 6C microstructural model.

Task 6D is a sub-task dealing with the tracer transport through a fracture network under site characterisation flow conditions. Simulated water residence time distribution varies from 110 hours to 180 hours and lengths of the flow paths are from about 60 m to 75 m. Transport modelling indicates that retention takes place mainly in the fracture coating. However, tracer release rates are controlled by the fault gouge, altered and unaltered rock. The role of the fault gouge indicates how sensitive is the overall retention on the geological and structural properties of the fracture wall rock. Fault gouge has an important role although it exists only along minor parts of the flow paths.

Task 6E is a sub-task that extends Task 6D from the site characterisation flow conditions to the performance assessment flow conditions. Tracer breakthrough curves are simulated for three different control planes that are placed at 10 m, 50 m and 130 m distances from the source location. Actual path lengths vary from 50 m to about 350 m

and water residence times from few years to about 150 years. Transport simulations of the Task 6E indicate that the fracture coating and fault gouge get saturated for all tracers already at the first control plane. Cataclasite and altered zone show clear indications of the limitation in the diffusion volume, but they are not fully saturated contrary to the fracture coating and fault gouge. This can be observed, for example, from the tailings of their contributions to the breakthrough curves, which do not follow the $t^{-3/2}$ power-law. The maximum release rate is controlled by the intact rock for all control planes.

Task 6F is a "benchmark" sub-task that studies contribution of the different fracture types to the tracer retention. Simulations are carried out for two single fracture cases: one with Type 1 fracture and another with Type 2 fracture. Water residence times are defined in the task definition to be between 0.1 years to 10 years and the distance between the tracer source and control lines is 20 m. The detailed description of the Task 6F makes it possible to concentrate only on the transport modelling and to derive the flow dependent transport properties directly from the task definition. Transport calculations show that the main difference between the fracture types is an additional delay in the breakthrough times for the transport through geologically complex fractures. The delay is caused by larger volumes of the high porosity immobile zones.

Task 6F2 is a collection of sensitivity analysis that studies different aspects of the transport processes in the fractured rock. Present modelling concentrates on the coupling of the flow and retention in the complex structure. Results of the Task 6F2 show that the retention by matrix diffusion is very sensitive to the flow rate. Flow path of the highest flow rate is very likely dominating the breakthrough curve. Retention and corresponding attenuation of the discharge rate is much smaller along the high flow rate flow paths than along the small flow rate flow paths. Task 6F2 simulations were performed using a system of two parallel fractures. The total flow rate is divided between the two fractures in different portions. Simulation results show that the flow path of higher flow rate dominates already when there is a factor of two difference between the flow rates.

Modelling of the Task 6 has indicated that retention in the site characterisation scale is easily dominated by geological materials that are small in volume but high in porosity, like the fault gouge. The importance of these materials in the PA scale may vary depending on the nuclide due to the sorption properties and radioactive decay (decay has not been considered in Task 6). It is likely that the geological materials, which have small volume, do not have such an important role in the PA than in the site characterisation.

Contents

List of Tables

List of Figures

1 Introduction

1.1 Background

Task 6 was initiated by the Äspö Task Force on Modelling Groundwater Flow and Transport. Task 6 is composed of several stages aiming to gradually increasing reality and complexity.

First subtasks, Tasks 6A, 6B and 6B2, were dealing with the transport along a single hydrological feature. They were modelled (Poteri, 2002) using a much simpler model than has been applied for the subtasks 6D, 6E, 6F and 6F2. The present transport model is able to take into account much greater number of details in the micro-structural model of the immobile pore space than the subtask 6A, 6B and 6B2 models. In practice, this means that the results of the earlier sub-tasks can not be directly compared with results of the sub-tasks 6D, 6E and 6F.

The present report describes Tasks 6D, 6E, 6F and 6F2 modelling as performed by the Posiva-VTT team.

1.2 Objectives

After Benabderrahmane et al. (2000) the overall objectives of Task 6 are to:

1. Assess simplifications used in PA models.
2. Assess the constraining power of tracer (and flow) experiments for PA models.
3. Provide input for site characterisation programs from a PA perspective (i.e., provide support for site characterisation program design and execution aimed at delivering needed data for PA).
4. Understand the site-specific flow and transport behaviour at different scales using SC models.

Most of the above objectives cannot be answered without modelling both SC and PA sides of the problem. The SC problem in the block scale is modelled in Task 6D. Block scale transport problem in PA conditions is modelled in Task 6E. Interpretation of the complex Task 6E required a series of “benchmark” runs on a simplified system. Task 6F consists of simulating flow and transport in a single Type 1 and a Type 2 feature, respectively. Additional Task 6F2 Sensitivity study is performed to exploit the model setup within Task 6E and 6F to perform additional studies evaluating specific topics of concern for the modelling of transport in fractured rock. The aim is to increase the understanding on how models behave, the reason for differences in modelling results, and the sensitivity of the models to various assumptions and parameter values. In the present report the Task 6F2 modelling is aimed to effects of flow in high complexity features.

1.3 Outline of report

Outline of this report follows recommendations of the Äspö Task Force group. Section 2 gives a short description of the modelling tasks and connection to the other tasks or experiments in the Äspö HRL. Section 3 gives a description of the applied modelling approach. Tasks 6D, 6E, 6F and 6F2 have been modelled using the same modelling approach, but the parameterisation varies between the sub-tasks. Simulated breakthrough curves are given in Section 4 and modelling results are discussed in Section 5.

2 Description of modelling tasks

2.1 Task 6

Benabderrahmane et al. (2000) defines Task 6 by stating that: “Task 6 tries to bridge the gap between PA and SC models by applying both approaches for the same tracer experiment, and also for PA boundary conditions.” This task is hoped to support PA calculations by identifying the relevant conceptualisations for longer term PA predictions and by identifying site characterisation data requirements.

In practice this means that modellers first implement their models such that they can reproduce the results from relevant Äspö in situ tracer experiments and then combines the use of PA and SC models for both PA and SC boundary conditions. Modellers can make appropriate assumptions for PA modelling, while continuing to honour the in situ tracer experiment result.

Task 6 is divided into several sub-tasks that proceed from simple and detailed configuration to more complex and comprehensive model:

Task 6A: Aim to model and reproduce selected TRUE-1 tests in a single water conducting feature.

Task 6B: Aim to model selected PA cases at the TRUE-1 site with new PA relevant (long term/base case) boundary conditions and temporal scales.

Task 6B2: Aim to apply different boundary conditions for the Task 6B feature, a complement of the Task 6B.

Task 6C: Aim to develop a semi-synthetic hydrostructural model in a 50-100m scale using data from the Prototype Repository, TRUE Block Scale, TRUE-1 and FCC.

Task 6D: Aim to model in-situ experiment in the block scale. Task 6D is similar to Task 6A, using the synthetic structural model and a 50 to 100 m scale TRUE-Block Scale tracer experiment.

Task 6E: Aim to model transport in block scale using PA time scales and boundary conditions. Task 6E extends the Task 6D transport simulations to PA flow conditions.

Task 6F: Aim to model a set of simplified “Test Bench” transport calculations. The system consists of a “building block” from the Task 6C model, i.e. a single feature of geological Structure Type 1 or Type 2, respectively.

Task 6F2: Aim to model sensitivity studies that exploit the model setup within Task 6E and 6F to perform additional studies evaluating specific topics of concern for the modelling of transport in fractured rock.

2.2 Task 6C semi-synthetic hydrostructural model

Modelling of the block scale transport, Task 6D and Task 6E, is based on a given geometry, hydrodynamic conditions and transport properties. Dershowitz et al. (2003) have developed a semi-synthetic hydrostructural model in Task 6C based on conditions at the TRUE Block scale site of the Äspö Hard Rock Laboratory. This model is built through a combination of deterministic and stochastic analyses of hydraulically significant structural features. The model contains 11 deterministic structures, 25 synthetic 100m scale structures and 5660 synthetic background fractures. At each scale, structures are described with regards to their geometric, hydraulic, and transport properties. Microstructural models are provided for the structures at each scale, including fault gouge, altered wall rock, and fracture coating.

The structures identified are attributed to two basic geological structure types; “Fault” (Type 1) and “Non-fault” (Type 2). A basic description and visualisation of the two types and their characteristic components (including intact unaltered wall rock, altered zone, cataclasite, fault gouge and fracture coating) are provided in Figure 2-1 and Figure 2-2. Geometric (thickness/extent) and transport (porosity, formation factor and K_d) parameters are assigned to the two types and given in Table 2-1.

In this study the semi-synthetic hydrostructural model is considered as the ultimate truth of the water conducting fractures in the modelling domain. It gives the exact locations, orientations and transmissivities of all fractures as well as the exact structure of the immobile pore space and sorption properties for the different types of groundwater. In the present study the modelling is made for the “TRUE Block Scale”-type of groundwater.

Due to the geological variability it is reasonable to assume that also the hydraulic and transport properties vary over the fracture. This is taken into account in the semi-synthetic model by introducing a complexity factor for each hydraulic structure. Complexity factor varies from 1 to 5. Larger values mean greater complexity and heterogeneity of the structure. In practice, the complexity factor distributes sub-parallel conductive features over the structure which leads to spatially variable transport properties. In this study the complexity factor is not taken into account. Structures are assumed to be spatially homogeneous and the micro-structural is entirely Type 1 or Type 2 over the whole feature.

Table 2-1. Geometric and transport parameters of the Type 1 and Type 2 fractures (from Dershowitz et al., 2003).

Type 1 (fault)			
Rock type	**Extent [cm]**	**Porosity [%]**	**Formation factor [-]**
Intact wall rock	-	0.3	7.3e-5
Altered zone	20	0.6	2.2e-4
Cataclasite dcat	2	1	4.9e-4
Fault gouge dg	0.5	20	5.6e-2
Fracture coating dc	0.05	5	6.2e-3
Type 2 (joint)			
Rock type	Extent [cm]	Porosity [%]	Formation factor [-]
Intact wall rock	-	0.3	7.3e-5
Altered zone	10	0.6	2.2e-4
Fracture coating	0.05	5	6.2e-3

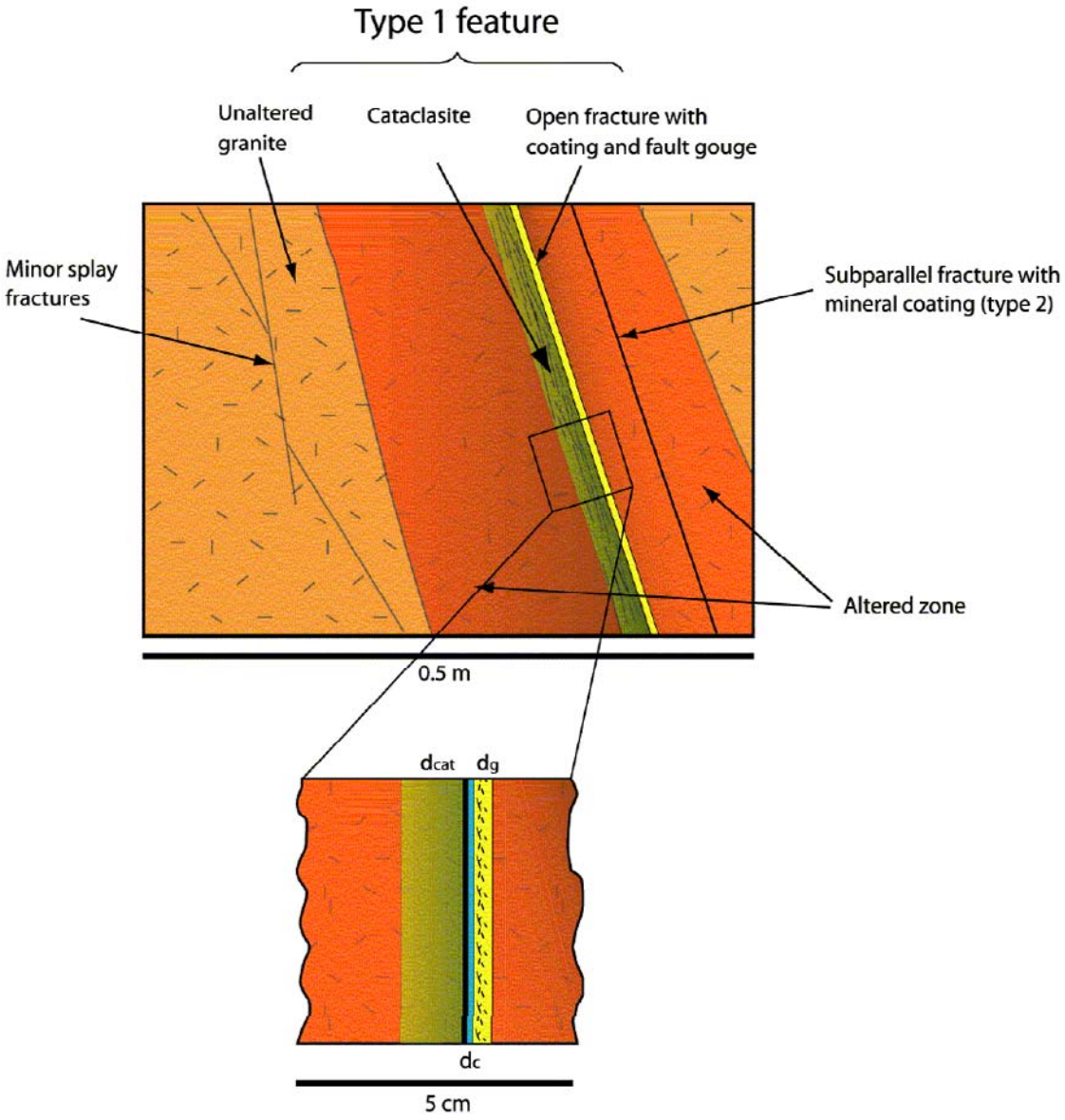

Figure 2-1. *Microstructural model of the Type 1 fracture as defined in the Task 6C semi-synthetic model (from Dershowitz et al., 2003).*

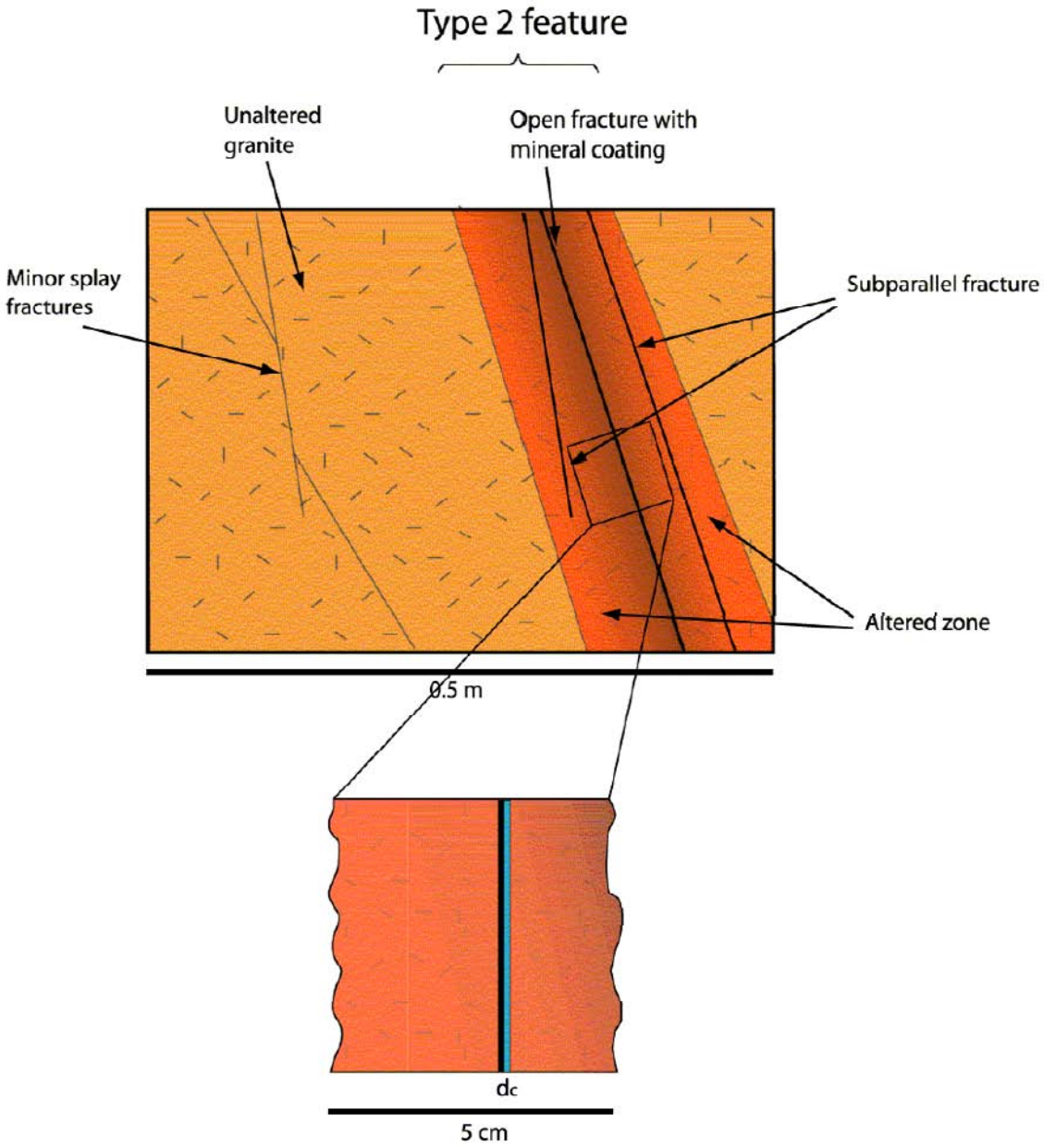

Figure 2-2. *Microstructural model of the Type 2 fracture as defined in the Task 6C semi-synthetic model (from Dershowitz et al., 2003).*

2.3 Task 6D

Task 6D focuses on solute transport over longer distances and transport paths that include several geological features are modelled. Detailed definition of the Task 6D is given by Elert and Selroos (2002). The basis for the modelling is the block scale semi-synthetic hydrostructural model developed within Task 6C (Dershowitz et al., 2003). In Task 6D this hydrostructural model is used to simulate tracer test C2 of the TRUE Block Scale tracer experiment. Task 6D provides a common reference platform for all SC-type and PA-type modelling in the considered block scale (200 m).

Time scale of the simulation corresponds to a few months to a few years (a tracer test scale). In Task 6D breakthrough of the tracers I-129, Ca-47, Cs-137, Ra-226, Tc-99 and Am-241 are simulated, although not all of these tracers were used in the actual TRUE Block Scale test C2. The purpose is to relate to the behaviour of radionuclides relevant for PA and in the case of Technetium and Americium also study how the retardation of more sorbing radionuclides can be extrapolated in time (Elert and Selroos, 2002).

Task 6D comprises of an extensive set of performance measures used to sort out reasons of the potential differences between different models. Majority of the performance measures are focused on the transport processes. They include breakthrough curves for different tracers and statistical measures of the breakthrough times. In addition to the measured injection curves, simulation results are requested for a Dirac pulse injection (unit input). This can support identification of the dominant retention processes in different modelling approaches.

2.3.1 TRUE Block Scale Tracer test C2

Tracer tests performed in the TRUE Block Scale covered a large span of distances (11 –130 m), both in a single feature and through a network of fractures (Andersson et al., 2002). Tracer test C2 tested flow path II of the TRUE Block Scale experiment. This flow path went through a network of fractures within Structures #23, #22 and #20. Calculated distance of this flow path along the interpreted deterministic structures was 97 m.

Tracer test C2 was performed using forced injection of 9 ml/min and extraction flow rate of 1960 ml/min (Andersson et al., 2002). Injected tracers contained a solution of ^{186}Re, ^{47}Ca, ^{131}Ba and ^{137}Cs. Non-sorbing ^{186}Re showed mass recovery of about 80% and ^{47}Ca showed mass recovery of 29%. More strongly tracers ^{131}Ba and ^{137}Cs did not have breakthrough during the monitoring time of about 5300 hours (Ba was followed only 3 months due to the short half life). Time of the first breakthrough of the ^{186}Re was at about 38 hours and the mean travel time was 282 hours (Andersson et al., 2002).

Andersson et al. (2002) conclude based on the evaluation modelling of the tracer test C2 that:

- The mean travel time and dispersivity is significantly higher than for a pathway through a simple structure.
- The model fit to the experimental data is not that good and the uncertainties in the parameter estimates are much larger than for the corresponding results for a pathway through a simple structure.
- Evaluated parameters indicating less retention than for a pathway through a simple structure.

2.4 Task 6E

Task 6E extends the Task 6D transport calculations to a reference set of PA time scales and boundary conditions. Detailed description of the Task 6E is given by Elert and Selroos (2004a). The basis of the Task 6E is the same Task 6C semi-synthetic hydrostructural model that has been applied also in the Task 6D.

Simulations of the tracer transport in Task 6E are calculated for the postclosure conditions. It is therefore not necessary to take into account the underground openings of Äspö HRL as was done in Task 6D.

The boundary conditions are simplified with fixed head boundary conditions at east and the west sides of the 200 meter block, while the other sides are treated as no-flow boundaries. The boundary conditions will give a gradient from east to west with a magnitude of about 0.5%. This corresponds to modelled gradients in the simulations of the Äspö site in SR 97 (Walker and Gylling, 1998). In Task 6D the gradient has been much higher. The background gradient, without pumping of the C2 test, is in the order of 10% calculated for the pumping and injection boreholes and using the Euclidean distance between them and with the pumping of the C2 test it is much higher.

The tracer source section has been chosen to be at the injection point of tracer test C2 in the deterministic feature 23D, i.e. at the same location as in Task 6D. This point is located near the centre of the 200m block. The source is assumed to be an intersecting fracture with a linear extension of 3 meters.

Tracer breakthrough curves are examined at three different locations. These are vertical north-south planes at easting=1880, easting=1920 and at the western boundary of the Task 6 block.

Task 6E simulations are performed using the same set of tracers as in the Task 6D, i.e. I-129, Ca-47, Cs-137, Ra-226, Tc-99 and Am-241. Performance measures of the Task 6E include also simulations for a Dirac pulse input (unit input) and an extend pulse of 1 MBq/year with a duration 1000 years.

2.5 Task 6F

The complexity in Task 6E makes it difficult to compare results of the different Modelling Groups. Task 6F is a series of “benchmark” runs on a simplified system that addresses the “building block” from the Task 6C model, i.e. the Geological Structures of Type 1 or Type 2, respectively. Detailed description of the Task 6F is given by Elert and Selroos (2004b).

The task consists of simulating flow and transport in a single Type 1 and a Type 2 feature, respectively. The features should follow the geometrical description from Task 6C and it is important to describe how the Task 6C model is implemented and what assumptions are made in the process. In Task 6F the modelled system is intentionally kept simple. Two features, Synthetic features 1S and 4S, are used in the Task 6F. They both have Complexity factor of 2 in the Task 6C model, but for the purpose of this exercise they are be considered to consist of a single fracture.

Hydrological properties of the features (Transmissivity, aperture, storativity) are taken from the Task 6C model. The modelling of the fracture surfaces and immobile zones follows the Geological types 1 and 2 defined in Task 6C (cf. Figure 2-1 and Figure 2-2). For the purpose of this exercise the fractures are assumed to have homogeneous properties according to Table 2-2.

Table 2-2. Properties of selected features (from Elert and Selroos, 2004b).

Structure Name	Width & Length	Geological Type	Complexity Factor	Transmissivity (m2/s)	Storativity	Aperture (m)
1S	112.44	1	2*	3.14E-07	2.80E-04	2.58E-04
4S	80.55	2	2*	1.90E-07	2.18E-04	2.01E-04

*For the purpose of this exercise considered to consist of a single fracture.

The boundary conditions are simplified with fixed head boundary conditions at two opposing boundaries of the selected features, while the other sides are treated as no-flow boundaries (Figure 2-3). The source term of the Task 6F is a Dirac pulse from a spatially extended source as shown in the Figure 2-3 and the breakthrough curves are calculated for a "collection line" at a distance of 20 meters from the source. Three different flow fields are simulated. The heads are adjusted to give an estimated groundwater travel times of 0.1, 1 and 10 years, respectively. The simulation cases and head differences required are presented in Table 2-3.

Task 6F uses a selection of tracers from Task 6E that includes I-129, Cs-137 and Am-241.

Table 2-3. Head boundary conditions for different cases (from Elert and Selroos, 2004b).

Case	Travel time (yr)	Head difference (m)	
		1S (Type 1)	4S (Type 2)
A	0.1	0.584 (case **A1**)	0.539 (case **A2**)
B	1	0.0584 (case **B1**)	0.0539 (case **B2**)
C	10	0.00584 (case **C1**)	0.00539 (case **C2**)

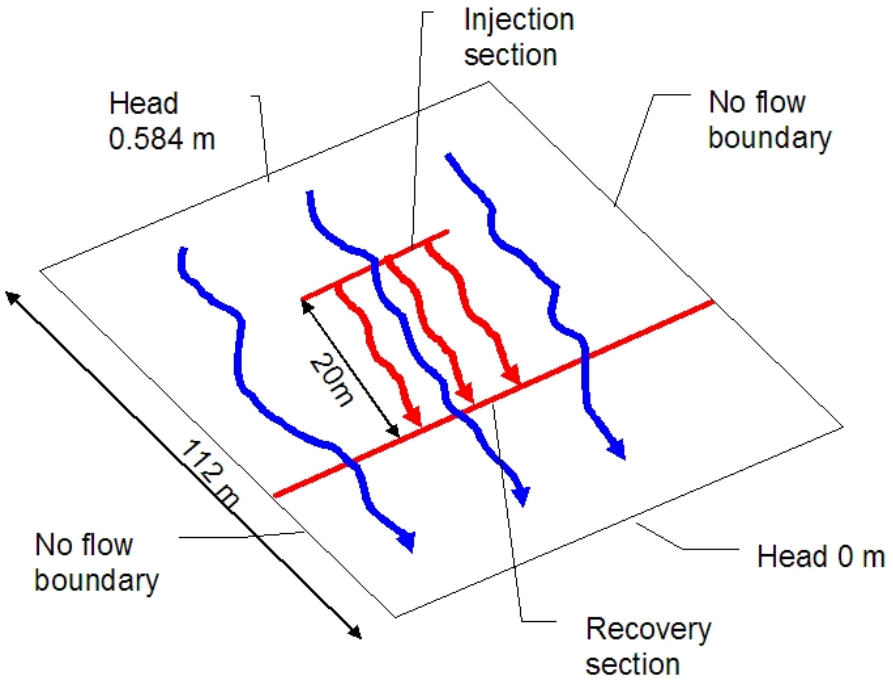

Figure 2-3. *Description of geometry and boundary conditions (Example for Case A1, from Elert and Selroos, 2004b).*

2.6 Task 6F2

Task 6F2 "Sensitivity analysis" studies the various aspects of the implementation of the Task 6C model. Task 6F2 investigates the model setup within Task 6E and 6F to perform additional studies evaluating specific topics of concern for the modelling of transport in fractured rock. Detailed definition of the Task 6F2 is presented by Elert and Selroos (2004c)

The aim of this task is to increase the understanding on how models behave, the reason for differences in modelling results, and the sensitivity of the models to various assumptions and parameter values. The proposed subtasks of the Task 6F2 are divided into the following categories:

1. The effect of flow on transport in low complexity features (single fracture),
2. The effect of flow on transport in high complexity features,
3. The effect of flow on transport in networks,
4. Additional tasks proposed by the Modelling Groups.

In the present report heterogeneity is studied by investigating coupling of the distribution of flow and retention in high complexity features (point 2 in the list above). The high complexity feature consists of several parallel conductive features that may also be of different geological type. The purpose of this subtask is also to study how the complex features should be implemented in SC and PA modelling.

3 Model description

3.1 Implementation of the Task 6C semi-synthetic hydrostructural model

Task 6D and 6E models attempts to follow the Task 6C semi-synthetic model as closely as possible. This applies both for the DFN model, i.e. for the hydrological active structures, and for the micro-structural model of the immobile zones in different fracture types.

The only feature of the semi-synthetic model that is not taken into account in the present Task 6D and 6E models is the complexity factor. It is assumed that all structures are homogeneous, there are no sub-parallel water conducting fractures inside the structures and the fracture type remains unchanged throughout the structure. This means that all hydraulic structures have only one water conducting fracture that is surrounded by the immobile zones according to the micro-structural model of that specific fracture type.

3.1.1 Geometrical description of fracture network

Geometrical description of the fracture network is based on the Task 6C semi-synthetic hydrostructural model. It contains 11 deterministic structures of the TRUE Block Scale site, 19 stochastic structures and 5648 background fractures. Characteristics of the fractures i.e. fracture locations, orientations, transmissivities, apertures and geological fracture types, are taken from the Task 6C semi-synthetic hydrostructural model.

3.1.2 Geometrical description of immobile pore space

The immobile pore space, as defined in Task 6C, is a stratified structure of different immobile layers. Task 6D and 6E models apply immobile pore space for both Type 1 and Type 2 fractures following the Task 6C specification as given in Table 2-1. Distribution of the immobile pore space for different fracture types is also illustrated in Figure 2-1 and Figure 2-2. Task 6D and 6E models assume that the different layers of the immobile pore space are homogeneous along the flow path as it is indicated in the Task 6C model (cf. Figure 2-1 and Figure 2-2).

The definition of the immobile pore spaces in Task 6C semi-synthetic model is asymmetric. The fracture coating as well as fault gouge exists only on one side of the fracture walls. However, an asymmetric structure of the immobile pore space can be represented by a symmetric system. Figure 3-1 shows how Type 1 and Type 2 microstructural models are represented by symmetric layers of the immobile pore space that will give an equivalent retention than the original asymmetric structure. The benefit of representing the microstructural model by the equivalent symmetric system is that we are able to apply the same solution of the advection-matrix diffusion equation throughout the modelling.

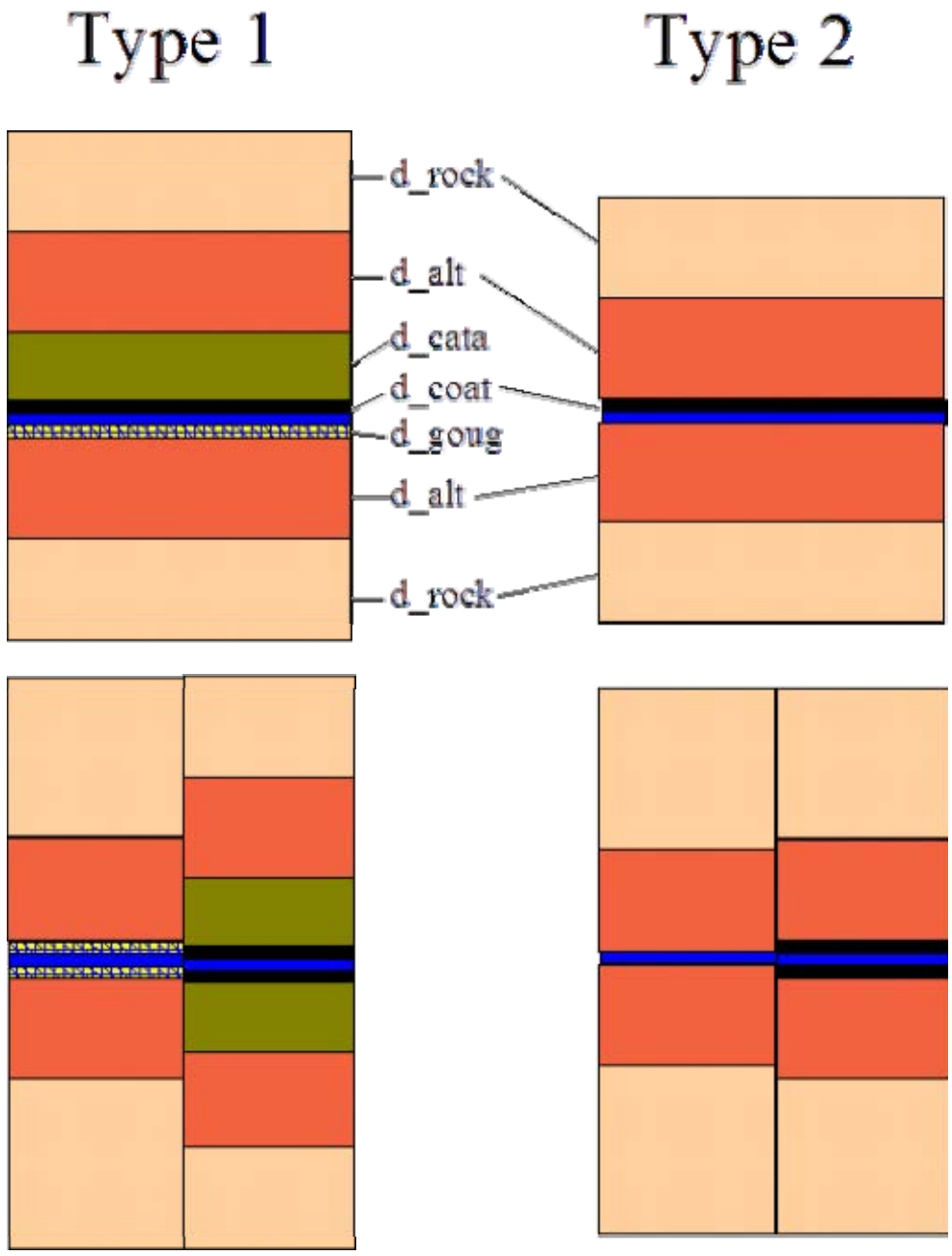

Figure 3-1. *Different layers of the immobile pore space as represented in the simulation model. Specification of the Type 1 and Type 2 structures in the Task 6C semi-synthetic model are shown at the top. The asymmetric distribution of the immobile pore space is represented in the model by two successive but symmetric structures of the immobile pore space as it is shown at the bottom of the figure. From the tracer retention point of view these two representations are equivalent.*

3.1.3 Descriptions for Task 6F and 6F2

Task 6F and 6F2 models apply the same microstructural model and modelling approach as Task 6D and 6E. The only difference is that in the Task 6D and 6E models the whole Task 6C fracture network is considered. Task 6F and 6F2 compare only individual Type 1 and Type 2 fractures.

3.2 Flow model

The flow model is based on the assumption that the water conducting fractures of the Task 6C semi-synthetic model are fully described by the transmissivities and fracture apertures. Transmissivity is used to calculate the volumetric flow rate through the fractures. The fracture aperture given in the Task 6C data delivery is used to calculate the advective transit times and in Task 6F and 6F2 also to evaluate the hydrodynamic control of retention (the F-factor).

3.2.1 Processes considered

Flow model describes the viscous flow of fresh water through the fracture network. Dissipation of the momentum in water and exchange of the momentum between the boundaries and the flowing water are taken into account by applying averaged dissipation of the energy, i.e. the concept of transmissivity. Relation between the flow rate, driving force and transmissivity is described by the Darcy's law.

Darcy's law with the equation of continuity indicate that the flow can be modelled using potential theory in which the potential to be solved is the hydraulic head.

3.2.2 Mathematical description

Groundwater flow is modelled in a steady state. The effect of salinity on the flow is not taken into account, but a constant fresh water density is assumed. The flow equation can be written as follows

$$\nabla \cdot \left(\mathbf{K} \nabla h \right) + Q = 0 \ , \qquad (3\text{-}1)$$

where h is the hydraulic head, $\mathbf{K}$ is the tensor of hydraulic conductivity and Q describes the sources and sinks in the model.

3.2.3 Numerical implementation

The flow equation (3-1) is solved numerically employing a conventional Galerkian finite element method. Modelling has been performed by applying the FEM code FEFTRA (2004).

In Task 6D and 6E all fractures of the Task 6C semi-synthetic hydrostructural model have been taken into account. They have been modelled as two-dimensional features by two-dimensional linear and triangular elements. The modelling domain is a cube that is located between easting of 1 800 and 2 000 metres, northing of 7 070 and 7 270 metres and elevation of -550 and -350 metres. The FEM model is composed of 68 235 triangular linear elements and 39 772 nodes. Resolution of the element mesh has been increased around the pumping and injection locations of the Task 6D and on the structures 20D, 21D, 22D and 23D. The mean element size is about 5.4 m, but on the structures 20D to 23D it is about 3.1 m. The same element mesh has been applied to model both Task 6D and 6E.

3.2.4 Parameters

Task 6D

Parameters of the flow model are based on the Data Delivery No 8 (revised features in 200 m scale model) and Data Delivery No 7 (boundary conditions for the 200 m scale model). Date Delivery No 8 includes geometries and transmissivities of all features. In the model they are applied directly as they have been specified in the data delivery.

The head boundary conditions on the external boundaries of the 200 m modelling domain have been assigned based on the given head values in the Data Delivery No 7. Prescribed head values on the external boundaries are represented for about 20 metres size panels. The prescribed head on the 20 metres panels is transferred on the outer boundary of the flow model by simply assigning the head value of the closest panel to each boundary node of the model. This gives a prescribed head boundary conditions on all external boundaries of the modelling domain. The applied boundary condition on the outer boundary of the Task 6D flow model is presented in Figure 3-2.

Extraction and injection flow rates provided in the Task 6D specifications are applied to the closest node points of the FEM model. The distance from the closest node point to the actual pumping location was less than 0.5 meters for both extraction and injection boreholes. The Task 6D pumping flow rates differ slightly from the actual pumping flow rates of the C2 test. Flow rates given by Elert and Selroos (2002) are applied in this model: extraction 1.95 l/min and injection 10 ml/min.

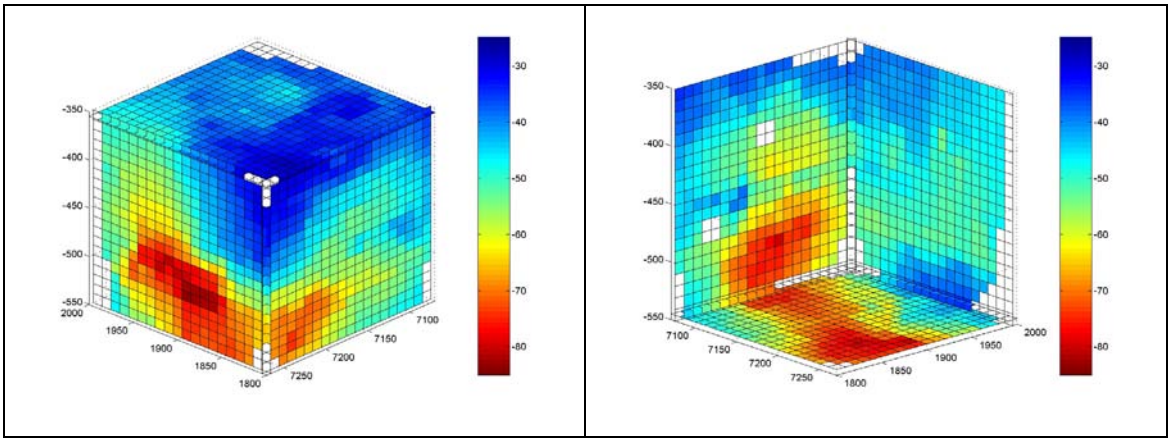

Figure 3-2. *Boundary condition applied on the outer boundary of the modelling domain is based on the Task 6C semi-synthetic model (the figure shows slices through the model, the outer boundary of the model is not completely flat and this results a few white "squares" in the figures).*

Task 6E

Parameters of the flow model in the Task 6E are based mainly on the data deliveries as Task 6D, i.e. the fracture network is defined in the Data Delivery No 8 (revised features in 200 m scale model). Naturally, boundary conditions for the Task 6E are different than in Task 6D. Prescribed hydraulic head of 0 m is applied at the Western boundary (X=1800) and hydraulic head 1 m at the Eastern boundary (X=2000). Other boundaries of the modelling domain are treated as no-flow boundaries.

Task 6F

Parameterisation of the flow field in Task 6F is very simple. Hydraulic properties of the two fractures examined in the Task 6F are given in the task definition (Elert and Selroos, 2004b). The Type 1 fracture has transmissivity of $3.14 \cdot 10^{-7}$ m^2/s and aperture of $2.58 \cdot 10^{-4}$ m. The Type 2 fracture has transmissivity of $1.9 \cdot 10^{-7}$ m^2/s and aperture of $2.01 \cdot 10^{-4}$ m. In the modelling the given apertures are treated as transport apertures of the fractures.

Task definition provides three different flow fields that are studied in Task 6F. The three different flow fields are specified to give groundwater transit times of 0.1 yr, 1 yr and 10 yr. Using the given apertures this can be used to directly calculate the $\beta = t_w / b$, where tw is the groundwater transit time and b is the half aperture (cf. also equation (3-5)). The β varies from about 780 yr/m to about 78 000 yr/m for the Type 1 fracture and from 1 000 yr/m to 100 000 yr/m for the Type 2 fracture.

Task 6F2

Parameterisation of the Task 6F2 is based on the Task 6F. The same two fractures as in the Task 6F are also used in the Task 6F2, but in this case they are parallel and the total flow is divided in different proportions between the two fractures. The total flow is the same for all calculation cases, only the division of the flow rate between the fractures changes. The used total flow rate corresponds to the flow rate through the Type 1 fracture in the case B1 of the Task 6F, i.e. the flow rate is about 5 litres/a over 1 meter wide section of the fracture (assuming the 20 m transport distance as in the Task 6F). In practice, the division of the total flow between the two fractures is accomplished by dividing the total β between the fractures. The total β used in the Task 6F2 simulations is about 7 700 yr/m.

Modelling of the Task 6F2 focuses on the retention properties of the fracture system. Therefore, no attention is paid on the advective delay and it is also omitted from the results.

3.3 Transport model

3.3.1 Processes considered

Transport model takes into account advection along the fractures, matrix diffusion and sorption in the immobile pore space. Surface sorption on the fracture walls is not modelled but the diffusion into the pore space of the fracture coating and sorption in the pore space of the coating is directly modelled.

Transport from source to sink is described by a set of transport paths that are determined using particle tracking. Inside a given transport path there is no variable advection but only a single flow velocity. Dispersion is not directly included into the model but the parallel transport paths through the flow model have different water transit times that cause route dispersion to the water transit time distribution.

3.3.2 Mathematical description

Transport of the tracers is described by applying the advection – matrix diffusion equation

$$\begin{aligned} R_a \frac{\partial c_f}{\partial t} + v\frac{\partial c_f}{\partial x} - 2\frac{D_e}{2b}\frac{\partial c_m}{\partial z}\bigg|_{z=0} &= 0 \\ R_p \frac{\partial c_m}{\partial t} - D_p \frac{\partial^2 c_m}{\partial z^2} &= 0 \end{aligned} \quad , \qquad (3\text{-}2)$$

where *Ra* is the retardation coefficient of the surface sorption (*Ra*=1 for all tracers in this modelling). Matrix concentration $c_m(x,z,t)$ and fracture concentration $c_f(x,t)$ are coupled by the requirement that $c_m(x,0,t) = c_f(x,t)$. Initial concentration is zero both in the matrix and in the fracture.

Laplace transform of the equation (3-2) gives

$$\begin{aligned} R_a s\,\bar{c}_f + v\frac{\partial \bar{c}_f}{\partial x} - 2\frac{D_e}{2b}\frac{\partial \bar{c}_m}{\partial z}\bigg|_{z=0} &= 0 \\ R_p s\,\bar{c}_m - D_p \frac{\partial^2 \bar{c}_m}{\partial z^2} &= 0 \end{aligned} \quad , \qquad (3\text{-}3)$$

where *s* is the variable of the Laplace domain. Equation (3-3) indicates that the solution could be sought using product $\bar{c}_m(x,z,s) = f(z)\bar{c}_f(x,s)$ with $f(0) = 1$. This leads to a solution

$$\bar{c}_f(x,s) = C_o \,\mathrm{Exp}\left(-\frac{R_a\, s\, x}{v} + \frac{2\,x\,D_e}{2b\,v} f'(0) \right) , \qquad (3\text{-}4)$$

where C_o is determined by the source term at the inlet of the flow path (e.g. for step input $c_o\,H(t)$, where *H* is the Heaviside's step-function, it is $C_0 = c_0 / s$. For the Dirac pulse injection $M_0\delta(t)$ it is $C_0 = \frac{M_0}{W(2b)v}\delta(t)$, where *W* is the width of the channel.). Boundary conditions of the immobile pore space are taken into account by the second equation of the (3-3) and they emerge into the solution of the breakthrough curve in the term *f'(0)*. For one homogeneous layer of immobile pore space we get

$$\begin{aligned} &\frac{2\,\varepsilon\,D_p}{2b\,v} f'(0) = \\ &= -2\sqrt{s}\,\frac{x}{v\,2b}\,\varepsilon\sqrt{D_p R_p}\,\tanh\left(L\sqrt{s\,R_p / D_p}\right) \\ &= -\sqrt{s}\,\beta\,\gamma\,\tanh\left(L\sqrt{s\,R_p / D_p}\right) \end{aligned} \quad , \qquad (3\text{-}5)$$

where $\beta = x/(v\,b)$ determines the flow conditions in the transport channel, $\gamma = \varepsilon\sqrt{D_p R_p}$ determines the properties of the immobile region and *L* is the thickness of the immobile pore space. This shows that two different immobile regions give the same retention (breakthrough curve) if they have the same γ and $L\sqrt{R_p / D_p}$, i.e. the same grouped matrix properties and the same "diffusion time" through the immobile layer.

Solute transport through the system of layered immobile zones is calculated by constructing an equivalent system of successive flow paths that have homogeneous immobile regions. This can be done if the diffusion property of the immobile layer is always smaller for the layer deeper in the rock matrix compared to the adjacent layer that is closer to the fracture. This is the case for the Type 1 and Type 2 features of the Task 6C semi-synthetic model and the modelled tracers. The immobile layers both in Type 1 and Type 2 features form a series of decreasing γ when the immobile layers are put in order from the fracture towards the intact rock. The modelling approach is explained below more in detail.

Let us consider a case where there are two different layers of the immobile pore space that differ only by the porosity (Figure 3-3a). We may conceptualise the connected porosity in the different immobile layers as 1D pipes that have different lengths (Figure 3-3b). Next, we may arrange the pipes along the flow path so that first are e.g. the short pipes then the longer pipes (Figure 3-3c). Changing the order of the pipes does not affect the solute transport, because if the flow path is composed of separate legs then the total output is a convolution between the outputs of the individual legs and convolution is a commutative operation. This means that a flow path with two layers immobile pore space could be modelled by a system of two successive flow paths that both have one layer of the immobile pore space according to Figure 3-3d. Note, that this is possible only if $\varepsilon_2 < \varepsilon_1$.

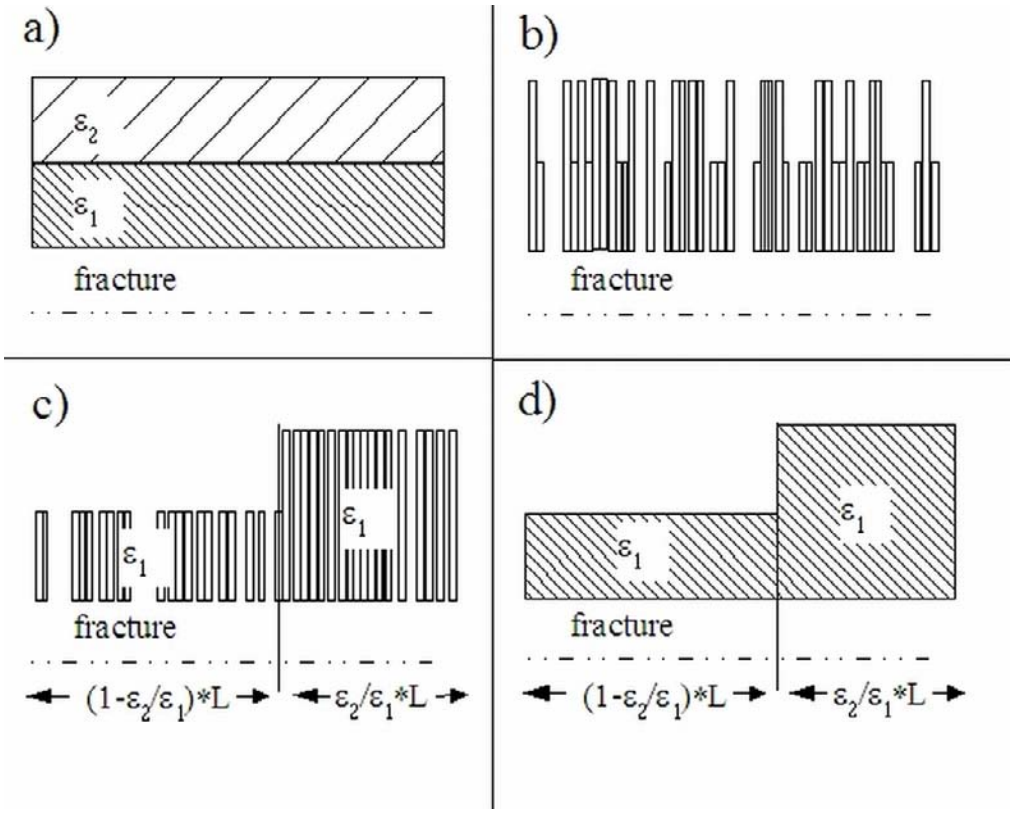

Figure 3-3. *Flow path along a fracture that is in contact with a heterogeneous immobile pore space. Immobile pore space is composed of two layers that have different porosities ($\varepsilon_2 < \varepsilon_1$, figure a). Connected porosity is represented by 1D pipes (figure b). The 1D pores are rearranged to form two successive legs of flow path that both have one layer of immobile pore space.*

The approach above can be extended to the cases where, in addition to the porosity, also diffusivity and sorption properties vary between the layers. According to the equation (3-5) the breakthrough curve depends on following parameters: β that describes the hydrodynamic control of the retention, γ that describes the properties of the immobile region and the "diffusion time" through the immobile layer, $L\sqrt{R_p / D_p}$. This means that the breakthrough curves for two flow paths are equivalent if they have the same β, γ and $L\sqrt{R_p / D_p}$, although the individual ε, D_p, R_p and L of the immobile regions are different. This is illustrated in Figure 3-4. It shows a breakthrough curve for a transport path that has groundwater transit time t_w=3 h and aperture 2b=1 mm. The immobile pore space and the tracers are described by two different sets of parameters so that γ and $L\sqrt{R_p / D_p}$ remain unchanged. Figure 3-4 shows that both parameterisations lead to the same breakthrough curves.

If we now have a transport problem with two layers of immobile regions such that $\gamma_2 < \gamma_1$, i.e. layer that is closer to the fracture has a bigger γ. We may now assign the same D_p and R_p for the second layer as for the first one but to remain the γ_2 unchanged we give a new porosity for the second layer such that $\gamma_2 = \varepsilon_2\sqrt{D_{p2}R_{p2}} = \varepsilon'_2\sqrt{D_{p1}R_{p1}}$. Changing D_p and R_p of the second layer will affect the "diffusion time" of the second layer if we do not at the same time change the thickness of the second layer by the factor of $\sqrt{D_{p1} / R_{p1}} \Big/ \sqrt{D_{p2} / R_{p2}}$. It was originally required that $\gamma_2 < \gamma_1$, which means that $\varepsilon'_2 < \varepsilon_1$. After these modifications the two layer case in which all parameters (D_p, R_p, ε and L) could vary between the layers is represented by, in the transport point of view, identical system where the two layers vary only by the porosity. This means that the procedure in Figure 3-3 is also applicable for the general case.

It is straightforward to take the next step to a system that contains several immobile layers. First, to apply this procedure the diffusion properties through the immobile layers should change such that $\gamma_m < \gamma_n$ if the layer *m* is further from the fracture than the layer *n* (Figure 3-5). Then we divide the flow path to as many legs as there are immobile layers. Starting from the layer that have the smallest γ (layer that is furthest from the fracture) we immediately see that the location of the leg *m* along the flow path is $[\gamma_{m-1}/\gamma_1, \gamma_m/\gamma_1] \cdot L$. The diffusion property of all legs is γ_1 and the thicknesses of the immobile layers are scaled by $L'_m = L_m \sqrt{D_{p1} / R_{p1}} \Big/ \sqrt{D_{pm} / R_{pm}}$ to keep the diffusion time unchanged (see Figure 3-5).

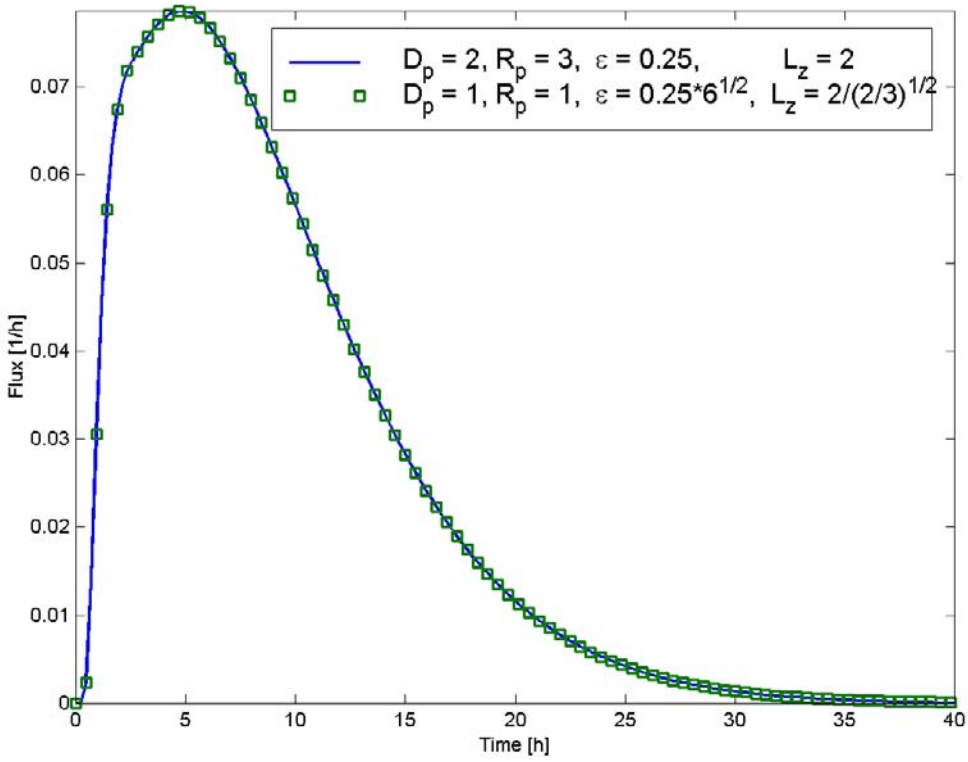

Figure 3-4. *Breakthrough curves for a transport path having properties t_w=1 h, 2b=1 mm and two different immobile layers. The results coincide because in both parameterisations* $\gamma = \varepsilon\sqrt{D_p R_p}$ *and the diffusion time through the immobile layer* $t_{diff} = L_z^2/(D_p / R_p)$ *remains unchanged. Note, advective delay is omitted.*

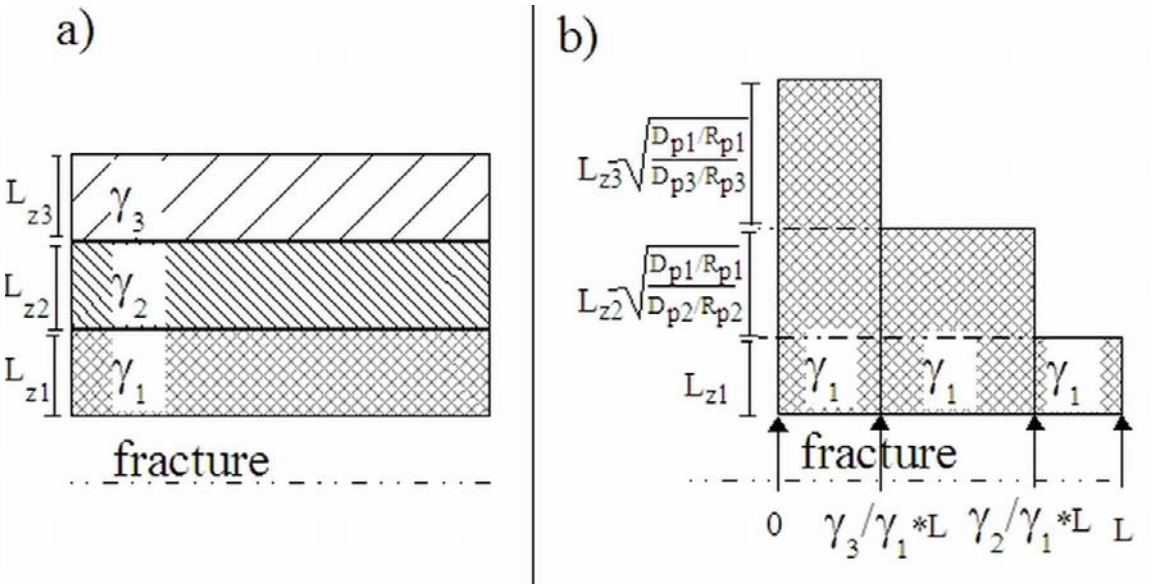

Figure 3-5. *A transport path with layered immobile pore space along the path (a) is divided into a sequence of flow paths that have homogeneous immobile pore space (b).*

3.3.3 Numerical implementation

Solute transport is calculated using an analytical model. Transport trough a flow path can be calculated by applying one-dimensional lattice walk where the exchange of the solute between the mobile and immobile pore spaces and possible interactions are described by the waiting time distribution (Cvetkovic and Haggerty, 2002). Our method is based on this approach. The waiting time distribution is calculated directly in the time domain and not in the Laplace-domain as it is done by Cvetkovic and Haggerty (2002).

The flow path is represented by 1D lattice. Discretization of the 1D lattice is performed so that convergent results are achieved but that on the other hand the calculation time is reasonable. In practice this means about 8000 grid points along each leg of the flow path. Figure 3-1 shows that a flow path through both Type 1 and Type 2 feature is represented by two legs that have symmetric matrix properties. Section 3.3.2 shows that both of these two legs, which are composed of layered immobile zones, are represented by a series legs of the flow path that have homogeneous matrix properties (cf. Figure 3-5). This means that e.g. the first part of the Type 1 feature in Figure 3-1 is represented by a series 3 legs of the flow path (gouge, altered rock, intact rock) and the second part by a series of 4 legs of the flow path (coating, cataclasite, altered rock, intact rock). This means that a flow path through Type 1 feature is represented by 7 different legs. Type 2 feature needs 5 legs, correspondingly.

Numerical calculations were carried using Matlab.

3.3.4 Parameters

Task 6D

Transport parameters are based on the data given in the semi-synthetic Task 6C model and presented in Table 2-1, which includes the geometrical and porosity data of the immobile layers. Tracer dependent data is also collected from the Task 6C model. Transport simulations are performed using sorption data of the TRUE Block Scale groundwater. Sorption properties for the additional tracers Radium, Technetium and Americium follow the recommendations in the Task 6C report. When calculating the retardation coefficients it has been assumed that all geological materials have the same density of 2600 m^3/kg.

Sorption and diffusion data set applied in the calculations is presented in Table 3-1. In addition, Table 3-2 shows the calculated γ values (cf. equation (3-5)) for the different layers and different tracers. It can be seen from the calculated values that the micro-structural model shown in Figure 3-1 does really have a sequence of decreasing γ from the fracture to the inner part of the matrix for all tracers, as it has been assumed in the applied modelling approach.

Table 3-1. Sorption and diffusion properties applied in the modelling for the different tracers.

K_d [m^3/kg]	I	Ra	Ca	Cs	Tc	Am
Intact wall rock	0	8.80E-03	4.40E-05	1.00E-02	2.00E-01	5.00E-01
Altered zone	0	1.80E-02	8.80E-05	2.00E-02	2.00E-01	5.00E-01
Cataclasite	0	1.30E-02	6.70E-05	1.50E-02	2.00E-01	5.00E-01
Fracture coating	0	4.60E-02	2.30E-04	5.20E-02	2.00E-01	5.00E-01
Gouge	0	1.40E-01	7.10E-04	1.60E-01	2.00E-01	5.00E-01
	I	**Ra**	**Ca**	**Cs**	**Tc**	**Am**
D_w [m^2/s]	2.00E-09	8.89E-10	7.93E-10	2.07E-09	5.00E-10	5.95E-10

Table 3-2. Matrix property γ calculated for different tracers and different geological materials. All tracers show a trend of decreasing γ from the fracture wall towards inner parts of the matrix.

γ [m $s^{-1/2}$]	I	Ra	Ca	Cs	Tc	Am
Intact wall rock	2.09E-08	1.22E-06	8.23E-08	1.98E-06	4.35E-06	7.5E-06
Altered zone	5.14E-08	3.02E-06	2.02E-07	4.85E-06	7.54E-06	1.3E-05
Cataclasite	9.9E-08	3.82E-06	2.66E-07	6.26E-06	1.12E-05	1.94E-05
Fracture coating	7.87E-07	2.5E-05	1.74E-06	4.06E-05	3.91E-05	6.75E-05
Gouge	4.73E-06	0.00012	8.63E-06	0.000196	0.000108	0.000186

Task 6E

Transport simulations in the Task 6E modelling are performed using the data as in the Task 6D modelling. Only the flow field has been changed from the site characterisation conditions of the Task 6D to the PA flow conditions of the Task 6E.

Sorption data of the tracers applied in Task 6E are presented Table 3-1 and the immobile zone retention properties in Table 3-2. Microstructural model of the Type 1 and Type 2 fractures follow the Task 6C model presented in Table 2-1.

Task 6F

Task 6F examines one Type 1 fracture and one Type 2 fracture. These fractures are selected from the Task 6C semi-synthetic model and therefore the microstructural model of the immobile pore space is identical with the Task 6D and 6E. The same parameterisation as in the Task 6D and 6E models is applied also in the Task 6F.

Sorption data applied in Task 6F is presented in Table 3-1 and the immobile zone retention properties in Table 3-2. Microstructural model of the Type 1 and Type 2 fractures follow the Task 6C model presented in Table 2-1.

Task 6F2

Task 6F2 examines complex structures under variable flow conditions. In the present Task 6F2 model this is conceptualised by a coupled system of one Type 1 and one Type 2 fracture. Microstructural model of the Type 1 and Type 2 fractures follow the Task 6C model presented in Table 2-1.

Sorption data applied in Task 6F2 follow the definition of the previous tasks and is presented in Table 3-1. The immobile zone retention properties are presented in Table 3-2.

3.3.5 Modelling strategy, model implementation and data selection

Task 6D

Transport modelling is divided into two parts. First, the flow dependent part of the transport properties, advective transit time and hydrodynamic control of the retention (β), are calculated using the flow model. This phase provides particle tracked transport paths and the corresponding transport properties.

Second phase of the modelling contains calculation of the tracer retention along the flow paths for different tracers taking into account matrix diffusion and sorption. Flow paths are treated as one-dimensional streamtubes and also the diffusion to the immobile zones is modelled as a one-dimensional process. This phase provides the breakthrough for a Dirac source term, without the advective delay, for each of the simulated flow paths and each of the tracers.

At the end, advective delay is added to the breakthrough curve of each of the flow paths and the breakthrough curves of all the flow paths are summed together to get the tracer breakthrough. Tracer breakthrough curve for a given source or injection function is calculated by convoluting the simulated breakthrough curve with the tracer injection curve.

Different modelling phases can be summarized by following stages:

- Building a FEM model that includes all features of the semi-synthetic Task 6C model.
- Steady state flow field is solved using the given boundary condition on the model boundaries and in the sink and source boreholes. The flow was solved using the FEM program package FETRA (FEFTRA, 2004).
- Flow paths are calculated by particle tracking through the calculated flow field. Matlab program is used to calculate the particle paths through the solved flow field. Possible flow paths are sampled by releasing 1000 particles. Each flow path is characterised by the integrated β along all Type 1 and all Type 2 fractures and by the water residence time along the flow path. It appeared that in the applied Task 6D model there is only 17 different pairs of β among the 1000 particle pathways. Pair of β means that each transport path is characterised by two β-values, one for the Type 1 fractures and another for the Type 2 fractures. This means that tracer retention is distinct only for 17 paths out of the 1000 paths simulated.
- Breakthrough curves are calculated using an analytical 1D model (cf. Section 3.3) and the 17 different simulated flow paths. At this stage the breakthrough curves do not yet include advective delay, but only retention caused by the sorption, matrix diffusion for a Dirac source term. Calculations are performed using a Matlab program.
- Advective delays are added to the breakthroughs.
- Breakthrough curves of all transport paths are summed together to get the tracer breakthrough curve. Breakthrough curves of the transport paths are weighted by the numbers of particles going through the route.
- Breakthrough curves for the given injection function are calculated by convoluting the simulated tracer breakthrough curves with the injection function.

Task 6E

The modelling strategy of the Task 6E modelling is essentially the same as in the Task 6D modelling. The main differences are that only 100 flow paths has been used in the Task 6E simulations, the flow field is different (cf. Section 3.2.4) and the performance measures are specified also for some intermediate locations along the release paths.

The source of the Task 6E is a 3 m long line source located in the centre of the Task 6 block. Starting points of the simulated 100 flow paths are selected randomly along the line source. In contrast to Task 6D all particle tracked flow paths give distinct transport properties. Individual transport paths are weighted by the flow rate at the starting point of the path. This indicates complete mixing or constant concentration along the line source.

Task 6F

The same modelling strategy as in the Tasks 6D and 6E is also applied in the Task 6F. This means that transport simulations are performed by applying analytical transport model based on the transport properties that are extracted from the flow model. In Task 6F the flow model is very simple. The task definition of the Task 6F provides all information that is needed for the transport calculations. In practice, modelling of the Task 6F is direct application of the transport model (Section 3.3) for the Type 1 and Type 2 fractures using the hydrodynamic control of retention given in the Section 3.2.4.

Task 6F2

Modelling approach of the Task 6F2 is identical with the Task 6F in a sense that there are only two fractures in the model. Flow is not modelled but different flow conditions are defined by directly parameterising the hydrodynamic control of retention. The flow system is composed of one Type 1 and one Type 2 fracture. The difference to Task 6F is that in Task 6F2 the total flow is divided between the two fractures. In Task 6F each of the two fractures are treated separately.

Transport through a high complexity feature is conceptualised by Figure 3-6. The total flow rate through a complex structure is divided between individual fractures and flow routes. Fractures in the high complexity feature have different retention properties, for example, the microstructural model of the fractures may vary.

Task 6F2 investigates a simple system that conceptually can be considered as a building block of the complex structures. This system is composed of two fractures that have different matrix properties. Theses two fractures form a system of two parallel flow paths as shown in the Figure 3-7. In Task 6F2 the division of the total flow between these two fractures is varied. It is also assumed that well mixed conditions prevails at the inlet of the system, i.e. the tracer mass through a fracture is proportional to the flow rate.

Task 6F2 modelling concentrates only on the retention properties. This means that advective delay is omitted in the results.

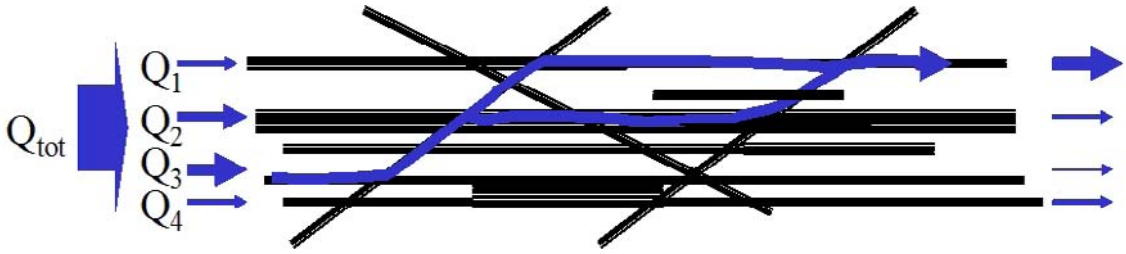

Figure 3-6. *Conceptual model of the complex structure. Black lines indicate fractures, blue lines are possible flow paths and the sizes of the blue arrows indicate flow rates.*

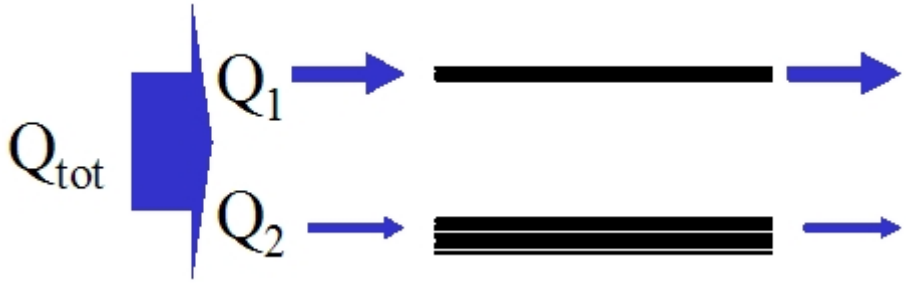

Figure 3-7. *A simplified model containing two fractures is studied in Task 6F2. One of the fractures is a Type 1 fracture and another is a Type 2 fracture.*

3.4 Model calibration and development

The selected modelling approach does offer many possibilities for the model calibration. The geometry and all physical properties of the structures are fixed by the Task 6C semi-synthetic model as well as the boundary conditions for the flow field. The Task 6C semi-synthetic model describes also the micro-structural model of all the structures and the properties of the tracers.

In principle, some calibration is possible in Task 6D that examines the tracer test C2 of the TRUE Block Scale experiment. In this case the calibration requires modifications e.g. to the defined micro-structural model. However, it is considered that transition from SC model (Task 6D) to the PA model (Task 6E) and comparison of between these sub-tasks is possible only if the Task 6C semi-synthetic model is treated as the “truth” of the DFN model (geometry, structure properties and micro-structural model) and that it is kept unchanged. This means that the focus of this work has not been in the interpretation of the in-situ experiments. The focus has been in the transition of the flow conditions from the in-situ conditions to the PA conditions and the corresponding changes in the major retention zones.

4 Results - Performance measures

4.1 Task 6D

4.1.1 Flow

Description of flow paths

Flow field is produced by the sink located in structure 21D and the given boundary conditions on the outer boundaries of the Task 6 modelling volume. Source of the tracers is located in structure 23D. Transport paths are sampled by 1000 particles that are released in the source borehole.

According to the particle tracking results flow paths visit structures 20D (900), 21D (1000), 22D (78), 23D (1000), 758C (134), 1925B (922) and 2403C (4), the number in parenthesis after the structure number shows how many of the 1000 particles visit the structure. Only the structure 20D is Type 1 feature, all others are Type 2 features.

The series of visited structures along the flow paths is called flow route in this report. Typically, in Task 6D a flow route contains four to five different structures. The flow routes are presented in Table 4-1 and in figures 4-1 and 4-2. Majority of the flow routes go through the background fracture 1925B. A small part of the flow goes also along the structure 20D.

Table 4-1. Flow routes represented by the series of the structures visited along the flow paths.

	Number of particles	Visited structures
Route 1	74	23D → 22D → 20D → 21D
Route 2	4	23D → 22D → 20D → 2403C → 21D
Route 3	100	23D → 1925B → 21D
Route 4	688	23D → 1925B → 21D → 20D → 21D
Route 5	134	23D → 1925B → 758C → 20D → 21D

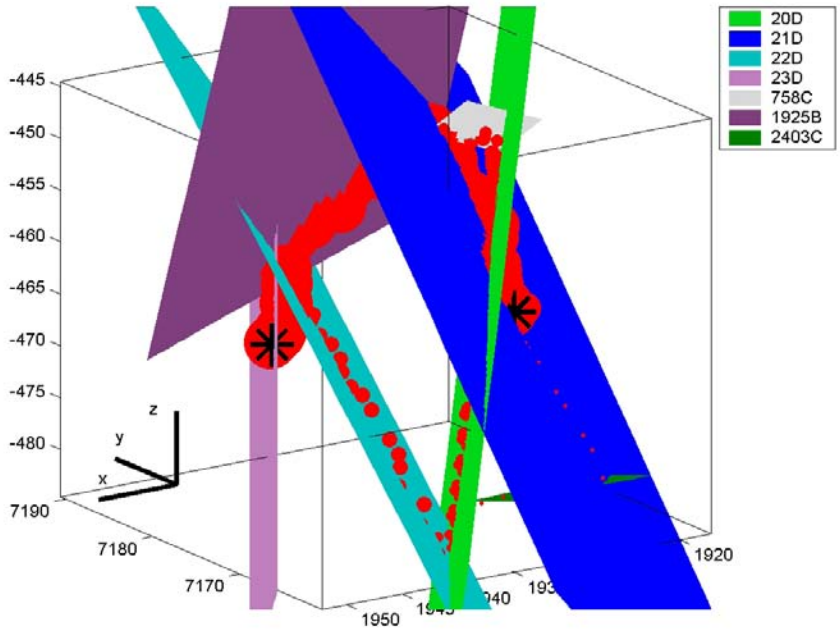

Figure 4-1. *Flow routes from the source to the sink are indicated by red dots. The size of the dot refers to the number of the particles that follow the route. The legend in the figure shows the colour coding of the structure numbers. The source and sink are indicated by black asterisks.*

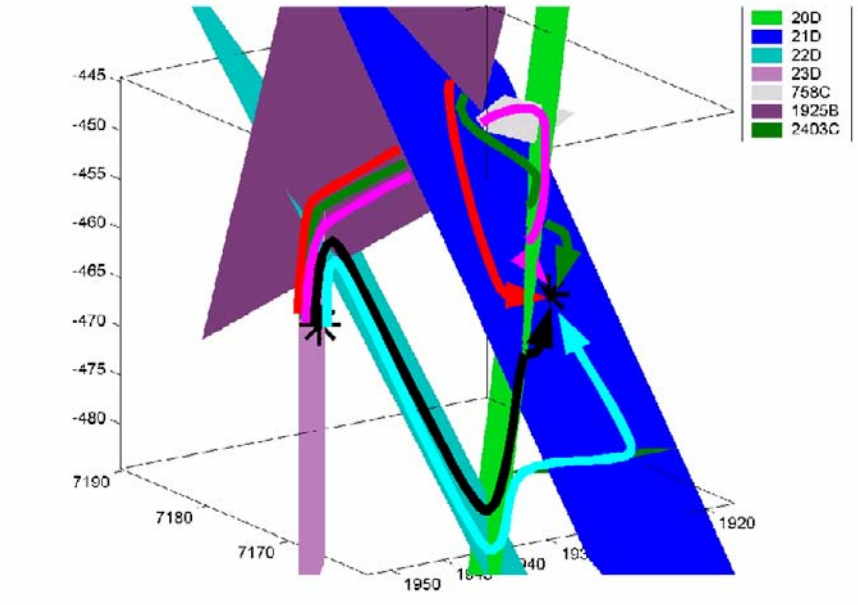

Figure 4-2. *Major flow routes indicated on the different structures. Structures that are visited along the different flow paths are presented also in Table 4-1. The same colour coding of the flow routes as in this figure is also used in the subsequent Task 6D figures.*

Drawdown in injection and pumping borehole

Drawdown in the injection and pumping boreholes is calculated by comparing the simulated hydraulic head values in the injection and pumping boreholes with and without the sink. This shows drawdown of 335 meters in the pumping borehole and 15 meters in the injection borehole.

Water residence time distribution

Groundwater residence times vary from 110 hours to 180 hours and correspondingly lengths of the flow paths vary between 59 and 74 metres (see Figure 4-3). Examination of the flow paths shows that there is some variation between the flow paths although all particles have started from exactly same location and the particle tracking through the flow field does not include molecular diffusion. Reasons for the variation is that well mixed conditions are assumed prevail at the fracture intersections. Next fracture is chosen randomly weighting the fractures by the flow rates assigned to them.

The water residence time distribution is presented in Figure 4-4.

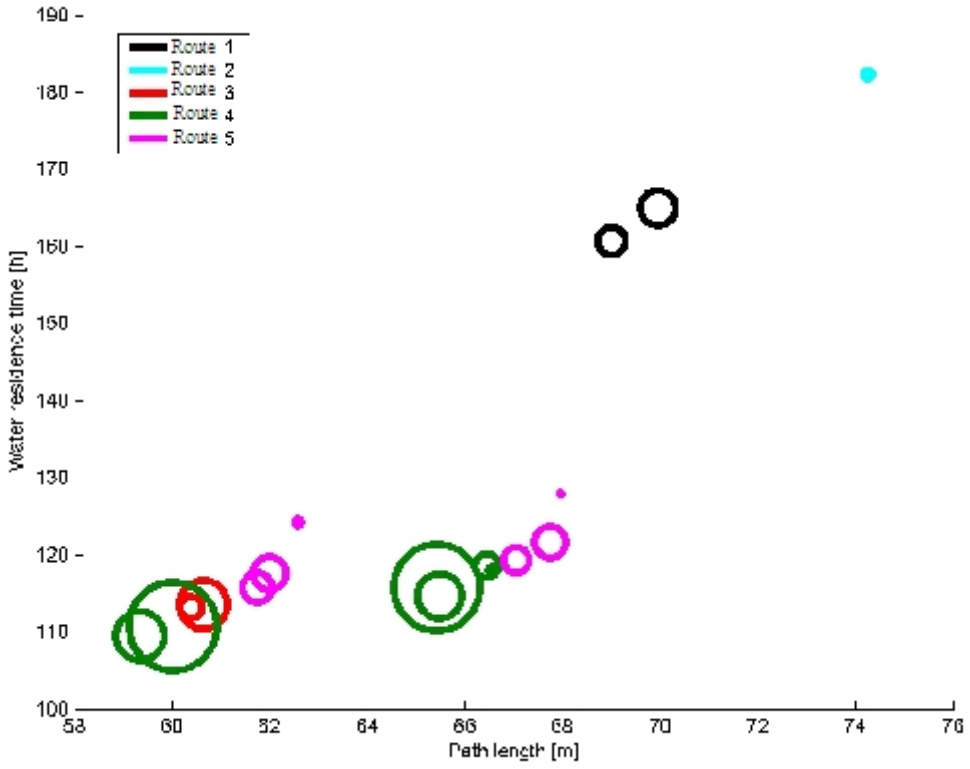

Figure 4-3. *Simulated Task 6D water residence times as a function of the path lengths. The size of the circle is proportional to the number of the particles along the flow route.*

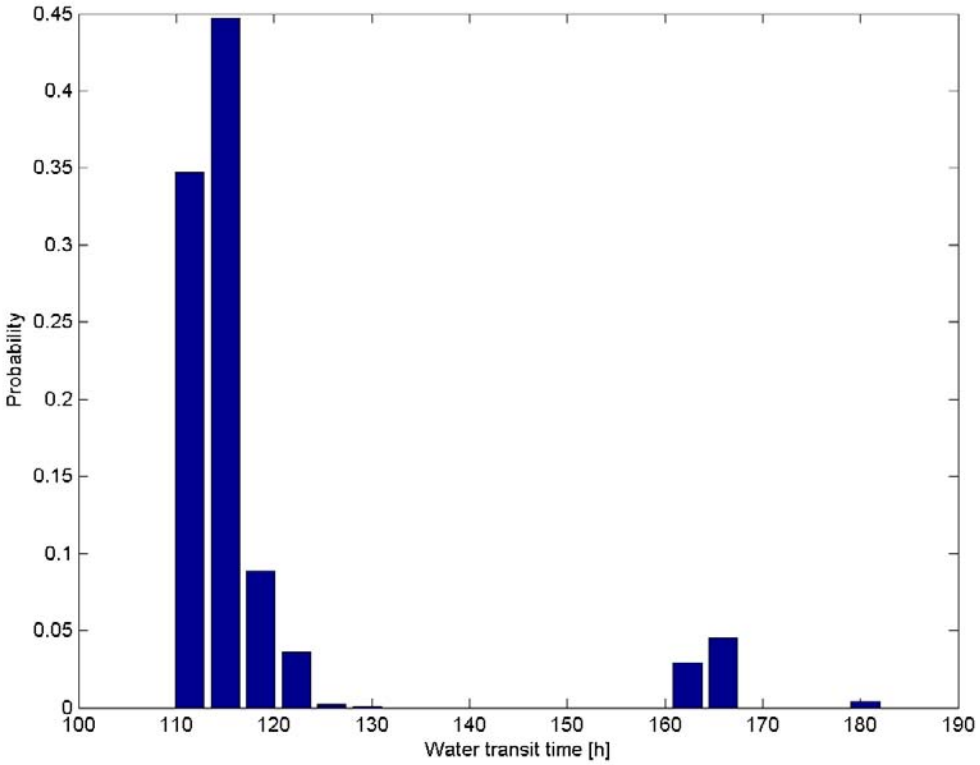

Figure 4-4. *Simulated Task 6D water residence time distribution.*

4.1.2 Transport

F-factor – ratio of flow wetted surface to water flow

The F-factor is identical with the β-factor used in this report. It is calculated as a part of the particle tracking simulations by applying equation (3-6)

$$\beta = \sum_i \frac{2 L_i}{q_i} \quad , \qquad (3\text{-}6)$$

where the sum i is made over all the elements in the FEM that the particle visits and $\beta_i = 2L_i/q_i$ is the contribution of the element i to the total β. Here, L_i is the length of the particle path over the element i and q_i is the Darcy velocity in the element i (i.e. Q/W, flow rate per fracture width).

Detailed investigation gives 17 different β-factors among the 1000 flow paths. The accumulation of the β-factor along the flow routes is illustrated in Figure 4-5. The solid lines show the cumulative β-factor as a function of the length of the flow path. Visited structures are presented by coloured circles at the background of the solid lines. From the slopes of the curves it can be concluded that strong retention (i.e. low flow rate along the flow path) takes place in structures 22D, 758C and 2403C. Especially, it may be noted that the β over the only Type 1 feature (20D) is quite small indicating relatively small overall retention in that structure.

The major flow route (route number 4, about 69% of the particles) shows β-factor ranging from 146 yr/m to 162 yr/m with mean value of 154 yr/m. For 92% of the particles β-factor is between 146 yr/m and 230 yr/m. Figure 4-6 shows the β-factor along all particle pathways sorted in the ascending order. The figure shows also contribution of the Type 1 and Type 2 features to the overall β-factor. Type 2 features are clearly dominating all paths, e.g. flow route number 3 goes entirely along Type 2 features. The flow route number 4 has the lowest overall β indicating high flow rate and correspondingly large number particles.

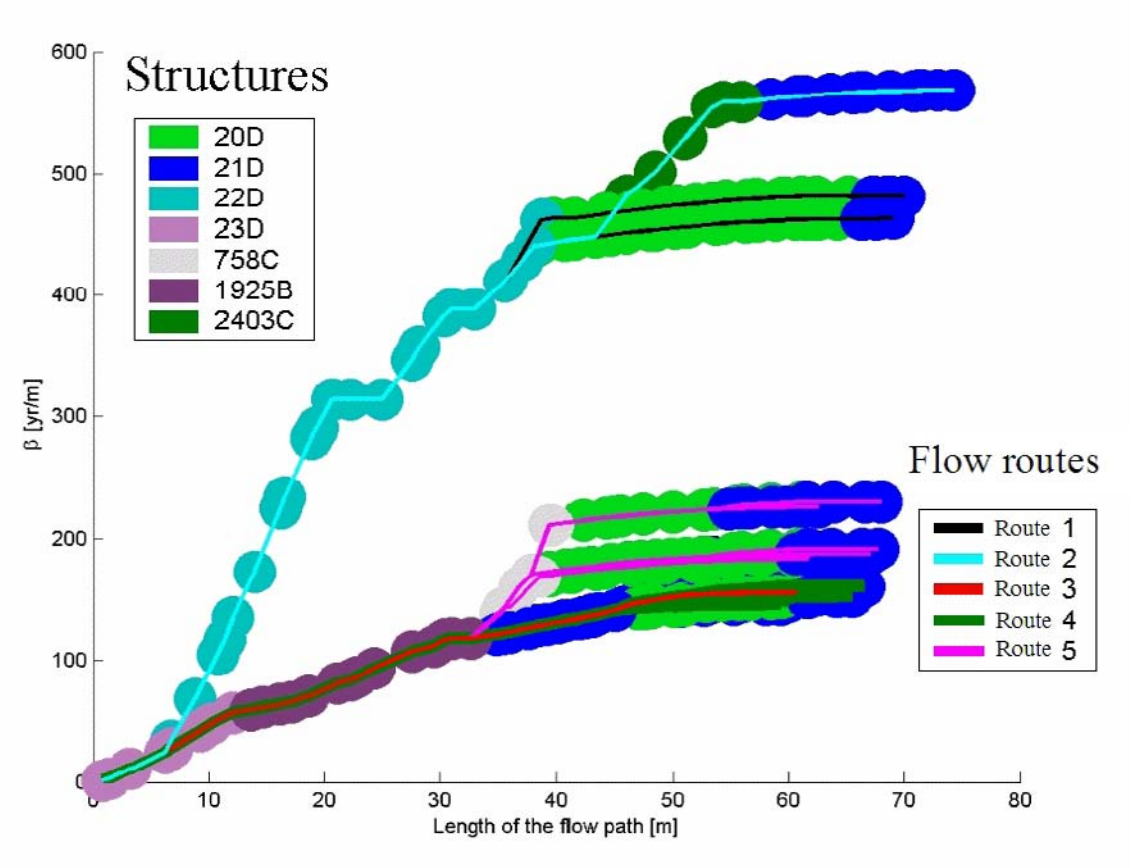

Figure 4-5. *Hydrodynamic control of the retention (β) as a function of the path length. Solid lines show β and the coloured discs at the background indicate the visited structures. The colouring of the paths and structures are the same as in the earlier figures. The major flow path (path number 4, solid green line) is plotted thicker than the others.*

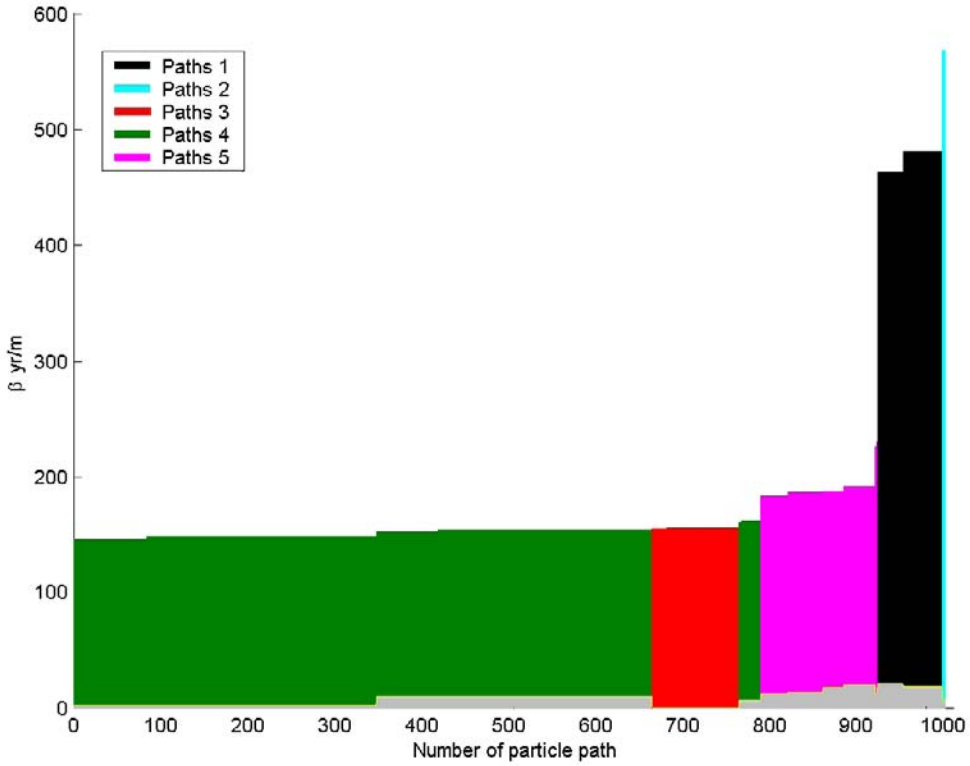

Figure 4-6. *Hydrodynamic control, i.e. β-factor, for all flow paths. Colours indicate the flow route. The x-axis shows the particle number (total of 1000 particles) and the y-axis shows the overall β-factor of the particle pathway. At each column the overall β-factor is divided between Type 1 structures (grey colour at bottom of the columns) and Type 2 structures (coloured with the colour of the transport route). Flow route 3 (red) is completely along Type 2 features. All other routes have also contribution from Type 1 features, but in many cases the contribution is so small that it is hardly visible in the figure.*

Breakthrough time history for the tracers

Calculated breakthrough curves for different tracers are presented below in Figures 4-7 and 4-8 and the corresponding breakthrough times in Tables 4-2 to 4-5. Breakthrough time histories for the Dirac pulse injection and for the measured injection function are quite similar. The reason is that the injection functions are quite narrow compared to the breakthrough curves. The half-widths of the source terms are in the order of few hours as they are hundreds of hours or more for the breakthrough curves.

Observed breakthrough curve for non-sorbing Re-186 in the TRUE Block Scale Test C2 shows peak time around 190 hours and the first breakthrough is around 40 hours. Task 6D simulations of the non-sorbing Iodine give first breakthrough around 130 hours and peak at about 150 hours. Simulated non-sorbing breakthrough curve seems to give reasonable mean travel time, but too narrow peak. This indicates that there is not enough interaction with the immobile pore spaces or the simulated flow field is not dispersive enough (note, that the transport model does not explicitly include dispersion). This can be seen also in the peak level of the release rates (Table 4-4 and Table 4-5). The observed level in the C2 test is about 6e5 Bq/h and the simulations give about 1.5e6 Bq/h.

Breakthrough curves for measured injection curves

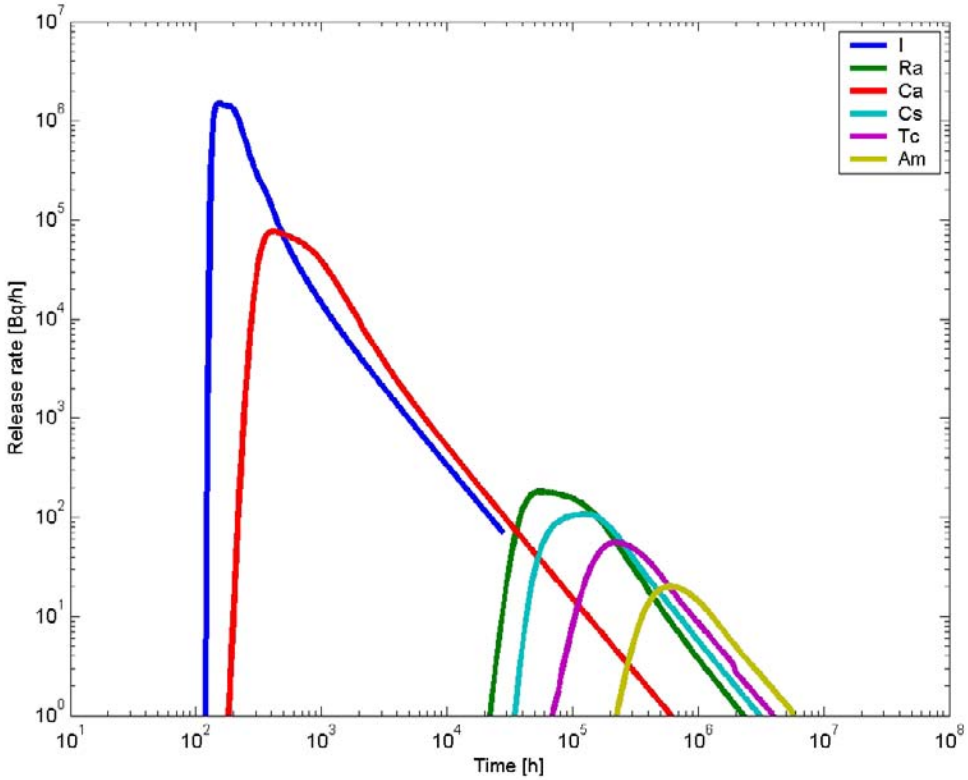

Figure 4-7. *Breakthrough curves for the measured tracer injection curves.*

Breakthrough times for recovery of 5, 50 and 95% of the injected mass.

Table 4-2. Breakthrough times for recovery of 5%, 50% and 95% of the injected mass.

	I-129	Ra-226	Ca-47	Cs-137	Tc-99	Am-241
t_5 [h]	1.44E+02	3.74E+02	7.76E+04	4.89E+04	1.68E+05	4.52E+05
t_{50} [h]	2.20E+02	1.06E+03	3.17E+05	1.81E+05	7.11E+05	2.00E+06
t_{95} [h]	3.41E+03	4.90E+04	2.79E+07	1.09E+07	6.85E+07	2.02E+08

Breakthrough curves for the Dirac pulse injection

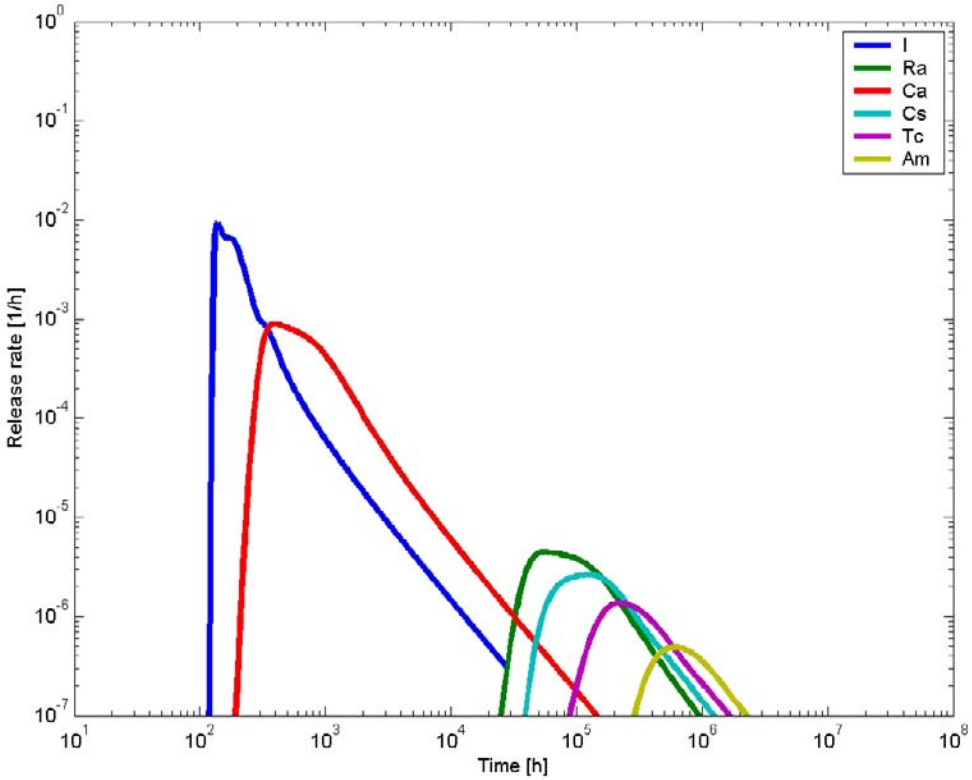

Figure 4-8. *Breakthrough curves for the Dirac pulse injection.*

Breakthrough times for recovery of 5, 50 and 95% of the Dirac pulse injection.

Table 4-3. Breakthrough times for recovery of 5%, 50% and 95% of the Dirac pulse injection.

	I-129	Ra-226	Ca-47	Cs-137	Tc-99	Am-241
t_5	1.36E+02	4.89E+04	3.62E+02	7.76E+04	1.68E+05	4.52E+05
t_{50}	2.01E+02	1.81E+05	1.05E+03	3.17E+05	7.11E+05	2.00E+06
t_{95}	3.40E+03	1.09E+07	4.90E+04	2.79E+07	6.85E+07	2.02E+08

Maximum release rate

Maximum release rate using measured injection curves

Table 4-4. Maximum release rate using measured injection curves.

	I-129	Ra-226	Ca-47	Cs-137	Tc-99	Am-241
Max. release rate [Bq/h]	1.51E+06	1.81E+02	7.62E+04	1.07E+02	5.57E+01	2.00E+01

Maximum release rate using Dirac pulse injection

Table 4-5. Maximum release rate using Dirac pulse injection.

	I-129	Ra-226	Ca-47	Cs-137	Tc-99	Am-241
Max. release rate [1/h]	9.41E-03	4.45E-06	8.99E-04	2.64E-06	1.37E-06	4.91E-07

4.2 Task 6E

4.2.1 Flow

Description of flow paths

Task 6E flow paths start from the middle of the modelling volume and are directed towards the northwest corner of the modelling volume. Transport of the tracers is examined at three different locations along the flow paths. These are vertical north-south planes located at easting=1880, easting=1920 and at the western boundary of the Task 6 block.

Flow paths are examined by particle tracking using 100 particles. Figure 4-9 shows the particle tracked flow paths by coloured dots. Each dot represents a FEM element visited by particles and the size of the dot indicates the number of particles visiting the element. The colour of the dot indicates the part of the flow path so that the red dots are used for the flow path from the source to the easting=1920, blue dots are used from the easting=1920 to the easting=1880 and black dots for the last part of the flow paths.

The main structures visited along the flow paths are shown in the Figure 4-10 and Figure 4-11. Figure 4-10 shows the major structures near the source and Figure 4-11 shows the structures that connect the flow paths to the boundary of the Task 6 block. Flow paths go mainly through seven different structures: 23D, 1925B, 20D, 21D, 22D, 17S and 2292B.

Particle path lengths from the source to the three sampling planes (easting=1920, 1880 and 1800) are presented in Figure 4-12. In some cases the particle pathway may intersect the sampling plane several times. Path lengths and corresponding water residence times are determined by the first intersection with the sampling plane.

The source is located approximately at the easting=1930. Path lengths from source to the first sampling plane are about 50 m to 100 m, although the Cartesian distance is only about 10 m. This follows from the subvertical orientation of the major structures that the particles follow.

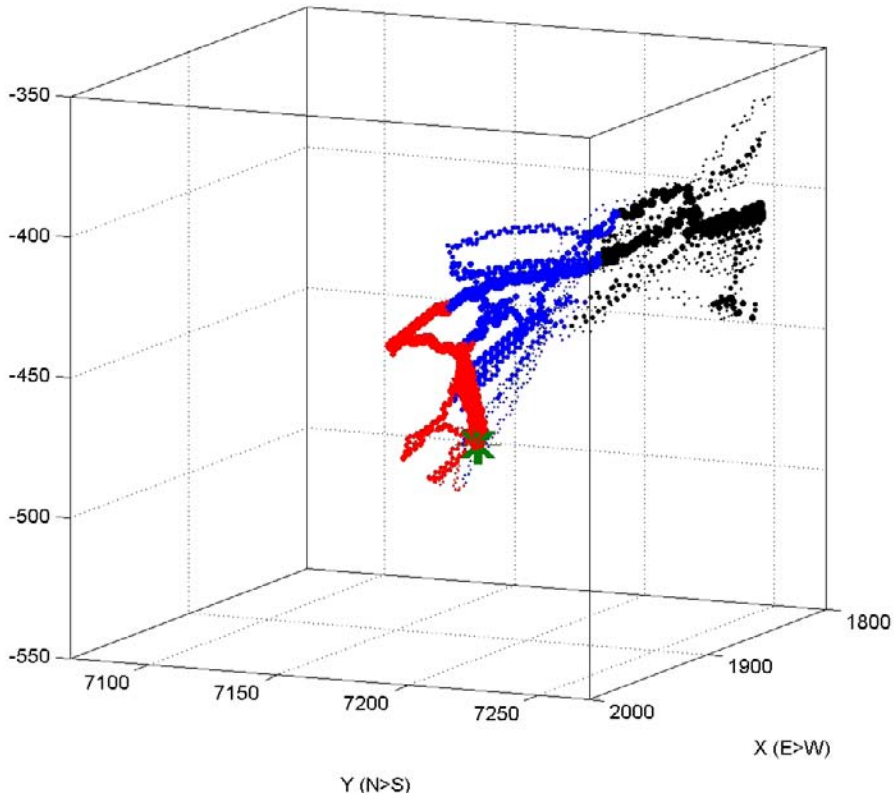

Figure 4-9. *Particle tracked flow paths are shown by coloured dots. Dots show the FEM element visited by the particles. Size of the dot indicates the number of particles that visit the element. Colours indicate different parts of the flow path: red is from source to easting=1920, blue from the easting=1920 to the easting=1880 and black from the easting=1880 to the boundary of the model. The source is marked by green asterisk.*

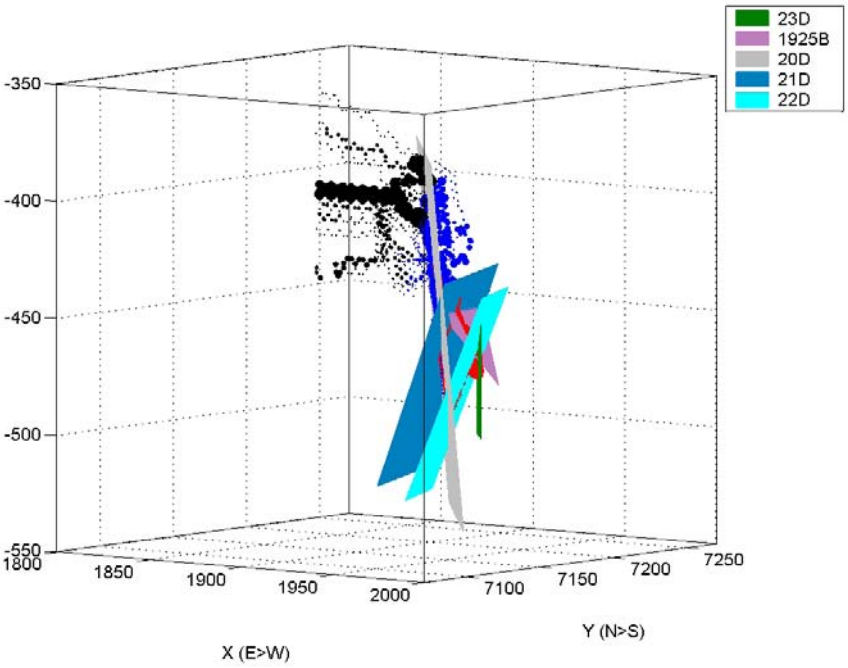

Figure 4-10. *The major structures visited by the flow paths at the vicinity of the source.*

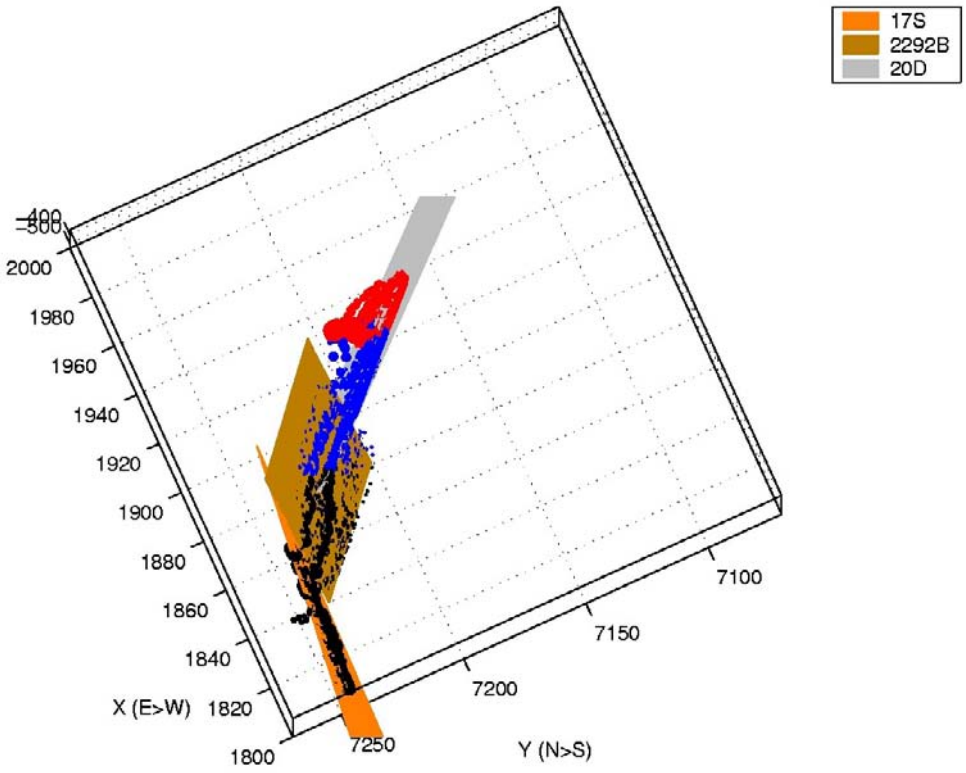

Figure 4-11. *The major structures connecting the flow paths to the western boundary of the Task 6 block.*

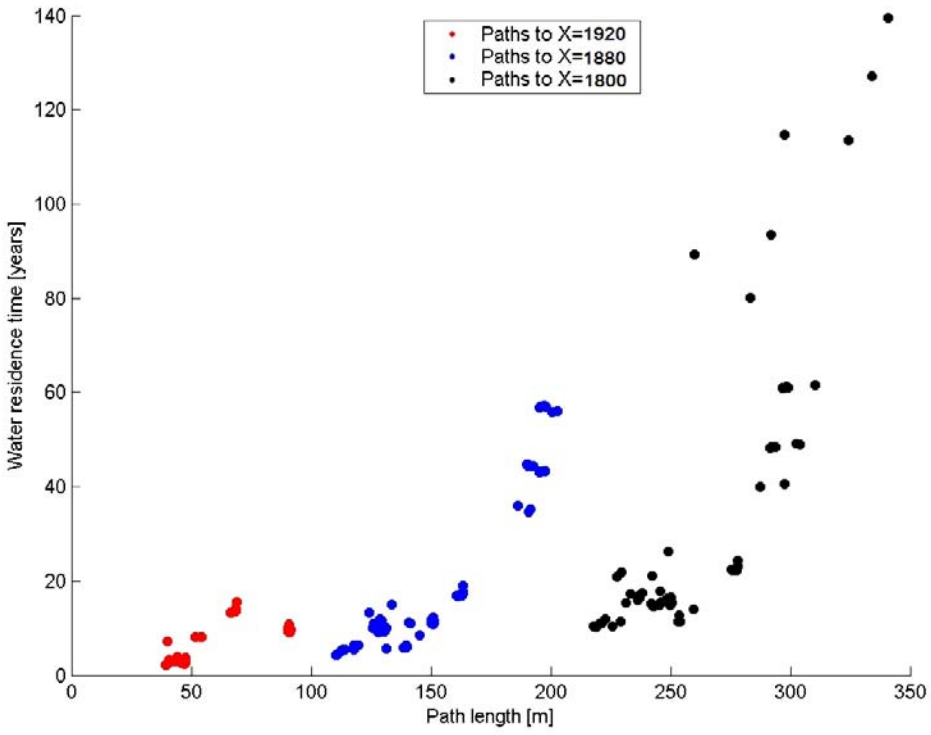

Figure 4-12. *Water residence times as a function of the path length at the three sampling planes. Cartesian distances from the source to the sampling planes are about 10 m, 50 m and 130 m.*

Water residence time distribution

Water residence time distributions at the three different sampling locations are presented in Figure 4-13. Comparison of the water residence time distributions shows that the major change between the different control planes is connected to the tailings. The spreading of the tailing of the breakthrough curve is much larger already at the 50 m distance than it is at the 10 m distance from the source. However, between distances of 50 m and 130 m the change is not that large. The route dispersion along the different flow paths is connected to the number of structures visited along the flow path. If the transport takes place through a single or only a couple of structures, then the route dispersion is moderate. This seems to be the case for the closest control plane.

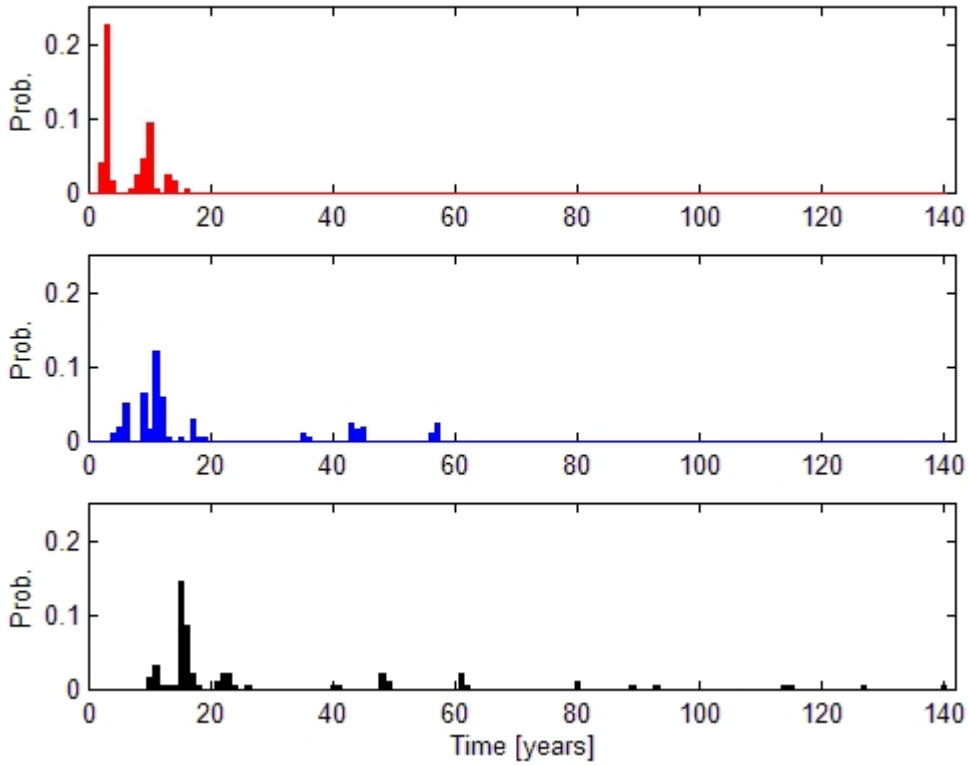

Figure 4-13. *Water residence time distribution from the source to the three different sampling planes (easting=1920 at top, easting=1880 in the middle and easting=1800 at the bottom).*

4.2.2 Transport

F-factor – ratio flow of wetted surface to water flow

As in the case of Task 6D the F-factor is given by the equivalent parameter β (Equation (3-6)). Hydrodynamic control of retention (β) along the all 100 tracked flow paths are presented in Figure 4-14 and Figure 4-15.

Table 4-6. Statistics of the β along the flow paths to the different control planes.

	Type	Min [y/m]	Max [y/m]	Average [y/m]
Easting 1920	Type 1	-	16 015	5 557
	Type 2	28 535	408 086	105 382
	Type 1+2	28 535	424 101	110 939
Easting 1880	Type 1	18 149	377 361	74 130
	Type 2	32 242	1 921 402	453 671
	Type 1+2	51 852	2 231 054	527 801
Easting 1800	Type 1	49 878	1 463 996	170 217
	Type 2	32 242	3 762 279	468 184
	Type 1+2	88 851	4 325 307	638 401

Figure 4-14 and especially Figure 4-15 show that for a large part of the flow paths the β does not increase much after the first sampling plane. It may indicate that those flow paths have reached well conducting hydraulic structures. Flow rates in these structures are large and correspondingly β is small. The same characteristic of the flow paths can be seen also in the Figure 4-16, which shows the accumulation of the β along the flow paths as a function of the length of the flow path. For large part of the flow paths the β does not increase after about 50 m path length. On the other hand, the spread between flow paths increases also considerably after the first 50-100 m. It is likely that the size scale of this behaviour is connected to the sizes of the hydraulic structures or fractures. The flat regions at the end of the flow paths also show the persistence of the flow paths to remain in the well conducting structures ones the flow path have entered the structure.

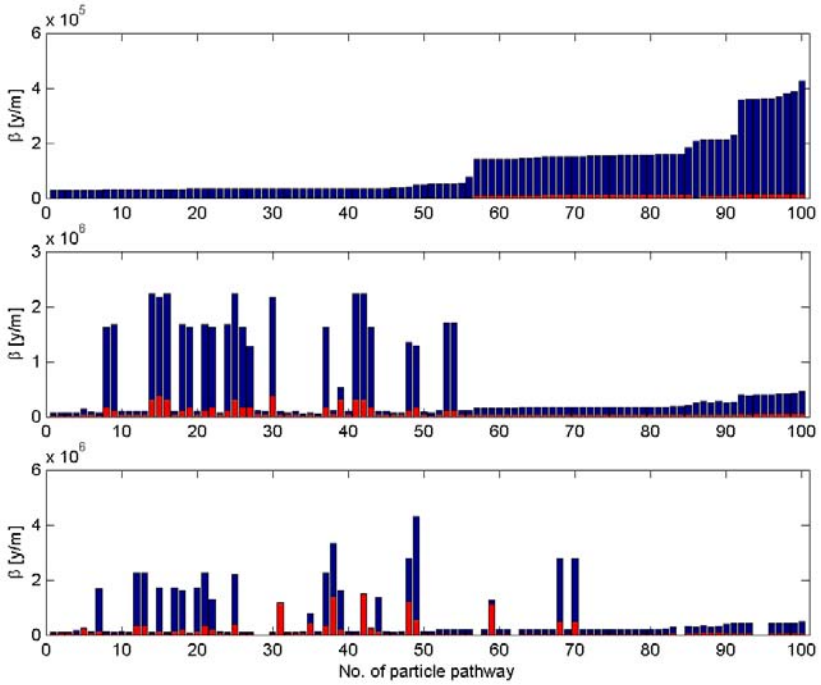

Figure 4-14. *The overall hydrodynamic control of retention (β) for all tracked particles. β is presented for the sampling plane at the easting=1920 (top), at the easting=1880 (middle) and at the easting=1800 (bottom). Height of the column indicates the total β along the path and the red part indicate contribution of the Type 1 fractures.*

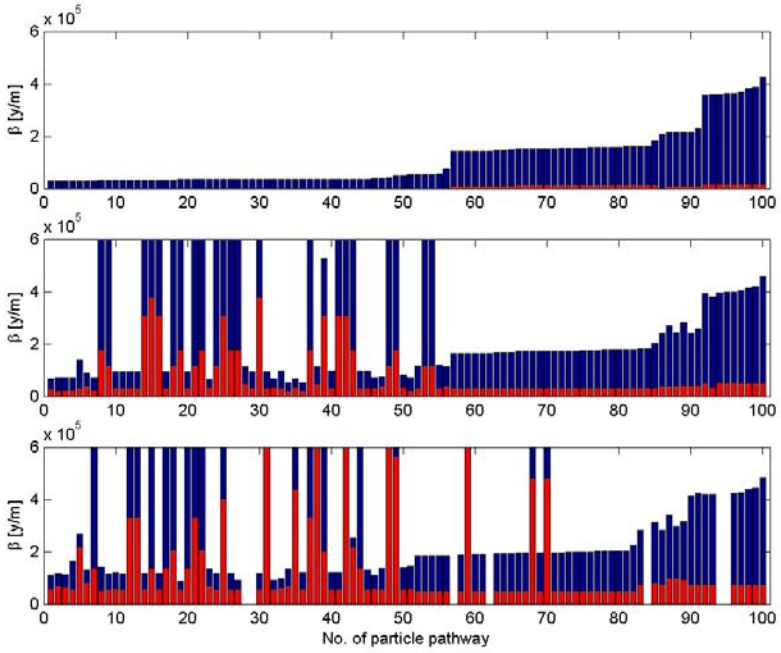

Figure 4-15. *The overall hydrodynamic control of retention (β) for all tracked particles. β is presented for the sampling plane at the easting=1920 (top), at the easting=1880 (middle) and at the easting=1800 (bottom). Height of the column indicates the total β along the path and the red part indicate contribution of the Type 1 fractures. This figure is the same as Figure 4-14, but in this figure the scale of the y-axis is same for all sampling planes.*

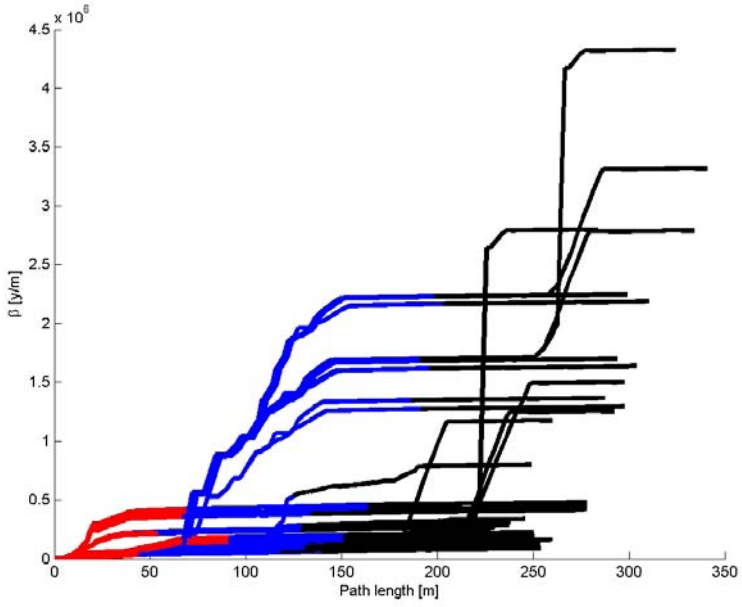

Figure 4-16. *Accumulation of the β along the particle pathways as a function of the path length. Red colour indicates particle paths from the source to the first sampling plane at the easting=1920, blue colour indicates paths from the easting=1920 to the easting=1880 and black colour indicates paths from the easting=1880 to the western boundary of the model.*

Breakthrough time history for the tracers

Breakthrough curves for a 1000 years injection of the 1 MBq/yr are presented in Figures 4-17 to 4-19 and the breakthrough times are given in Table 4-7. Breakthrough curves for the Dirac pulse injection source term are presented in Figures 4-20 to 4-22 and the corresponding breakthrough times are given in Table 4-8.

In some of the cases the breakthrough curves show a double peak behaviour, especially this can be seen in the Dirac pulse injection breakthrough curves for the first control plane, e.g. Figure 4-20. The two peaks are produced by the two main flow routes, which have a little bit different flow properties.

Breakthrough curves for extended injection

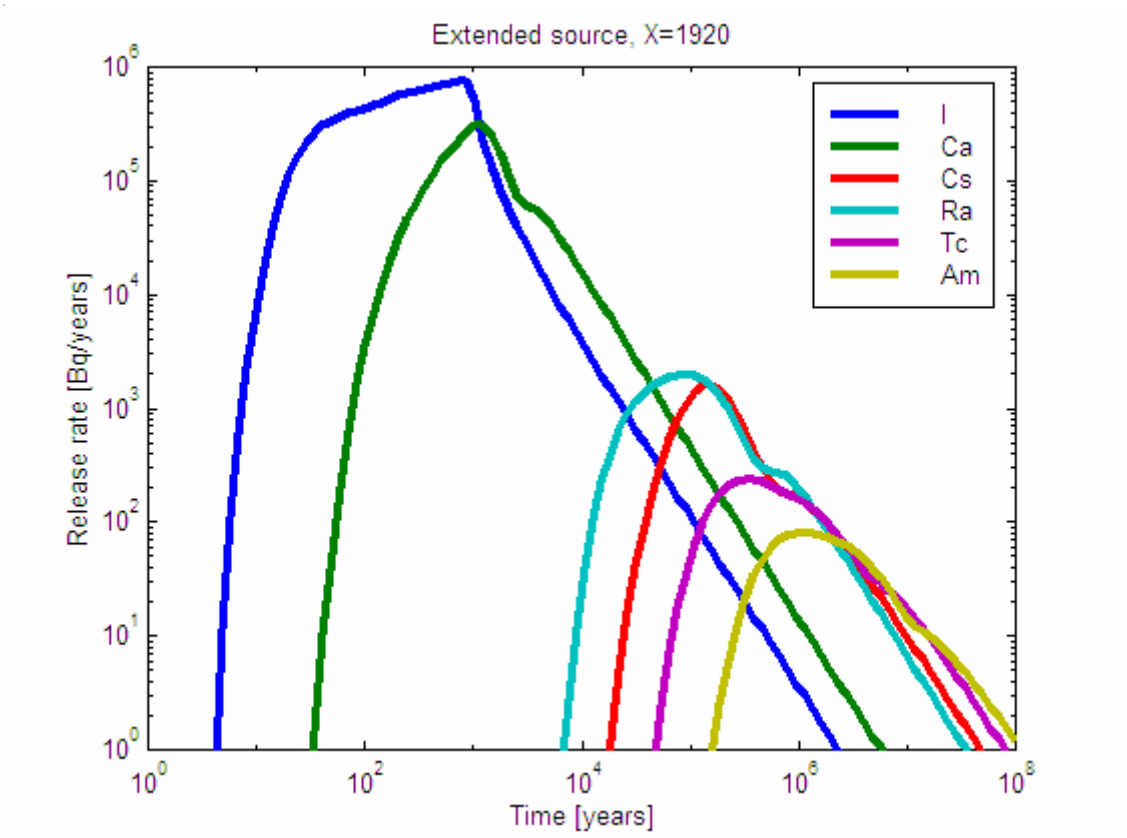

Figure 4-17. *Breakthrough curves at easting=1920 for the extended 1000 years source of 1 MBq/yr.*

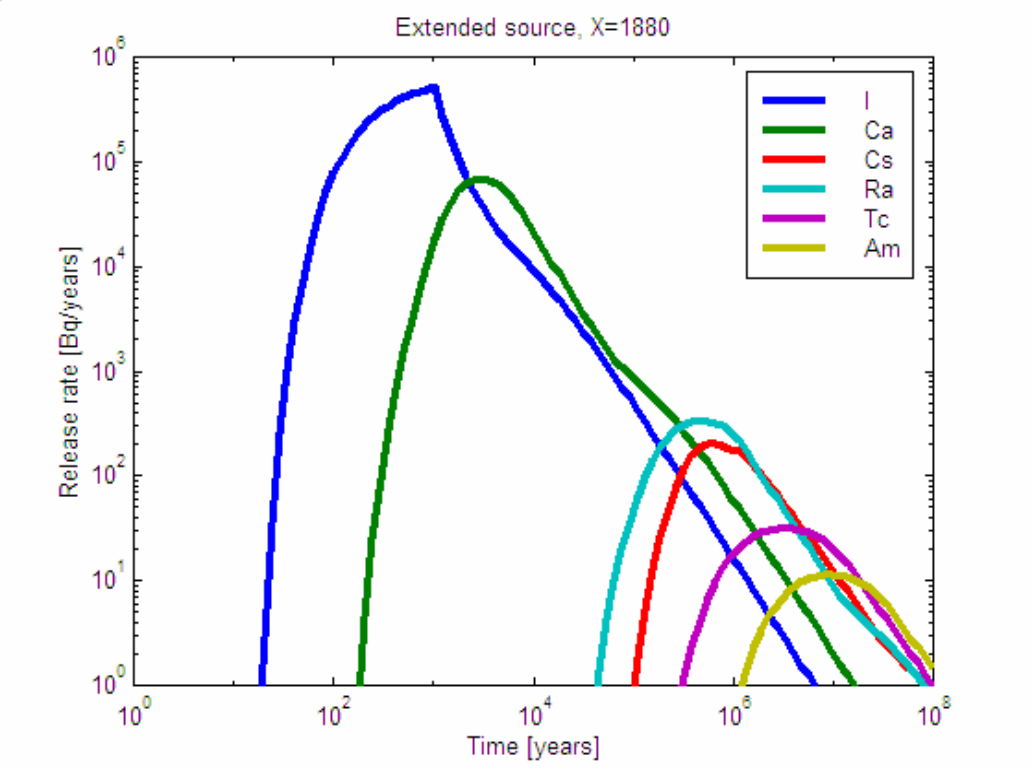

Figure 4-18. *Breakthrough curves at easting=1880 for the extended 1000 years source of 1 MBq/yr.*

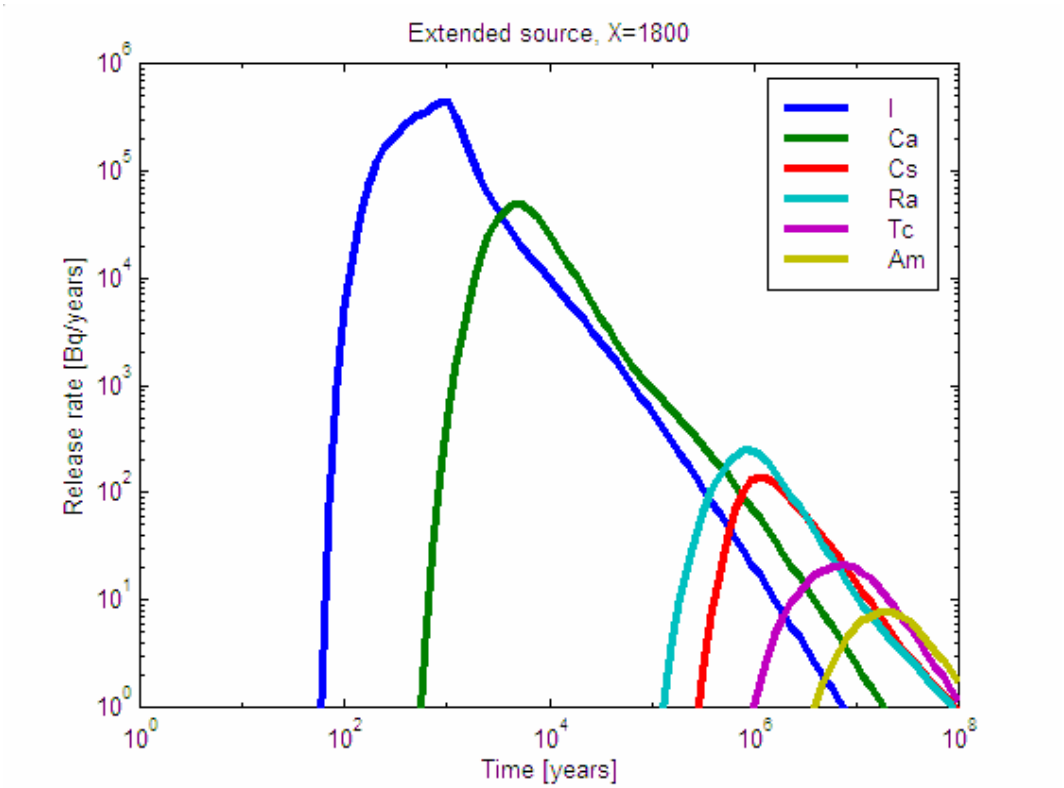

Figure 4-19. *Breakthrough curves at easting=1800 for the extended 1000 years source of 1 MBq/yr.*

Breakthrough times for recovery of 5, 50 and 95% of the injected mass for the extended injection

Table 4-7. Breakthrough times at the different control planes for the 1000 years injection of the 1 MBq/yr.

Easting=1920						
	I	**Ca**	**Cs**	**Ra**	**Tc**	**Am**
t_05 [y]	144	605	91740	53 570	321 900	944 100
t_50 [y]	724	3 039	1 130 000	551 300	5 674 000	16 640 000
t_95 [y]	21 850	385 100	>1E8	48 810 000	>1E8	>1E8
Easting=1880						
	I	**Ca**	**Cs**	**Ra**	**Tc**	**Am**
t_05 [y]	295	1 775	460 800	321 900	2 314 000	6 788 000
t_50 [y]	1 240	15 270	6 788 000	3 313 000	34 100 000	>1E8
t_95 [y]	321 900	4 742 000	>1E8	>1E8	>1E8	>1E8
Easting=1800						
	I	**Ca**	**Cs**	**Ra**	**Tc**	**Am**
t_05 [y]	353	3 039	944 100	551 300	4 742 000	13 910 000
t_50 [y]	1 775	26 140	11 630 000	4 742 000	58 390 000	>1E8
t_95 [y]	551 300	9 717 000	>1E8	>1E8	>1E8	>1E8

Breakthrough curves for Dirac pulse injection

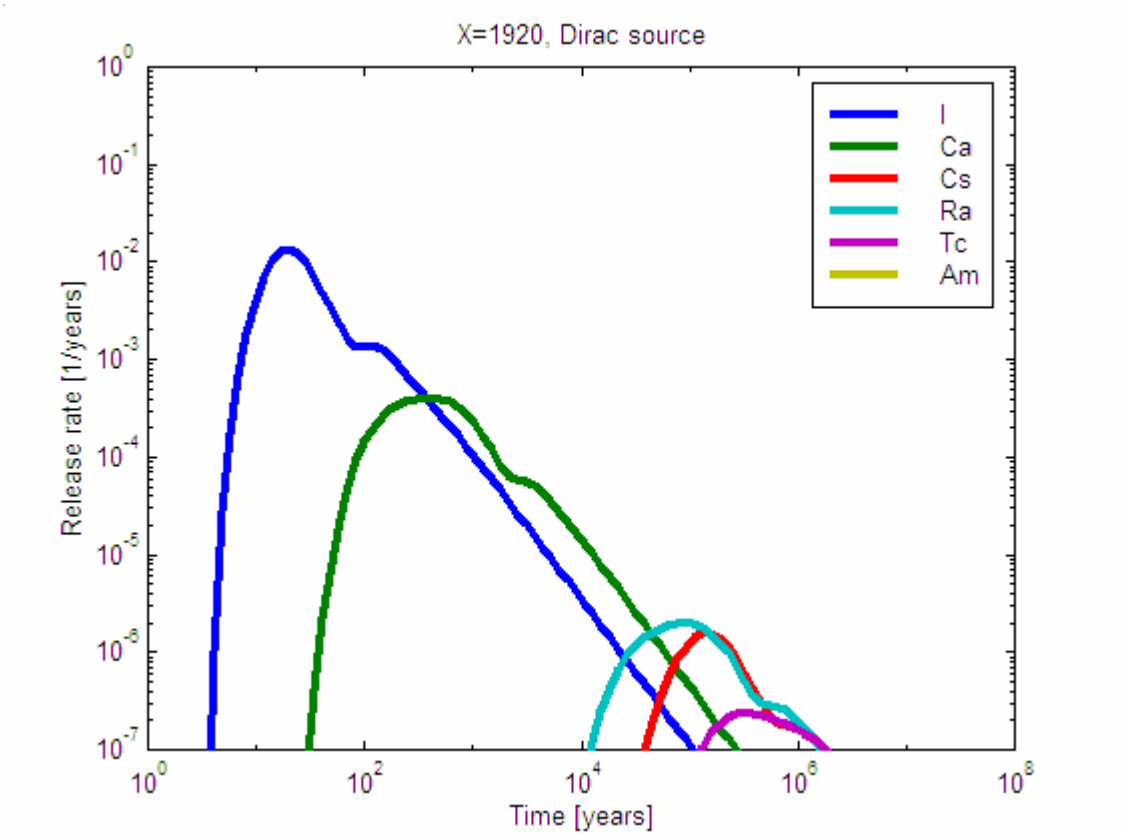

Figure 4-20. *Breakthrough curves at easting=1920 for the Dirac pulse injection source term.*

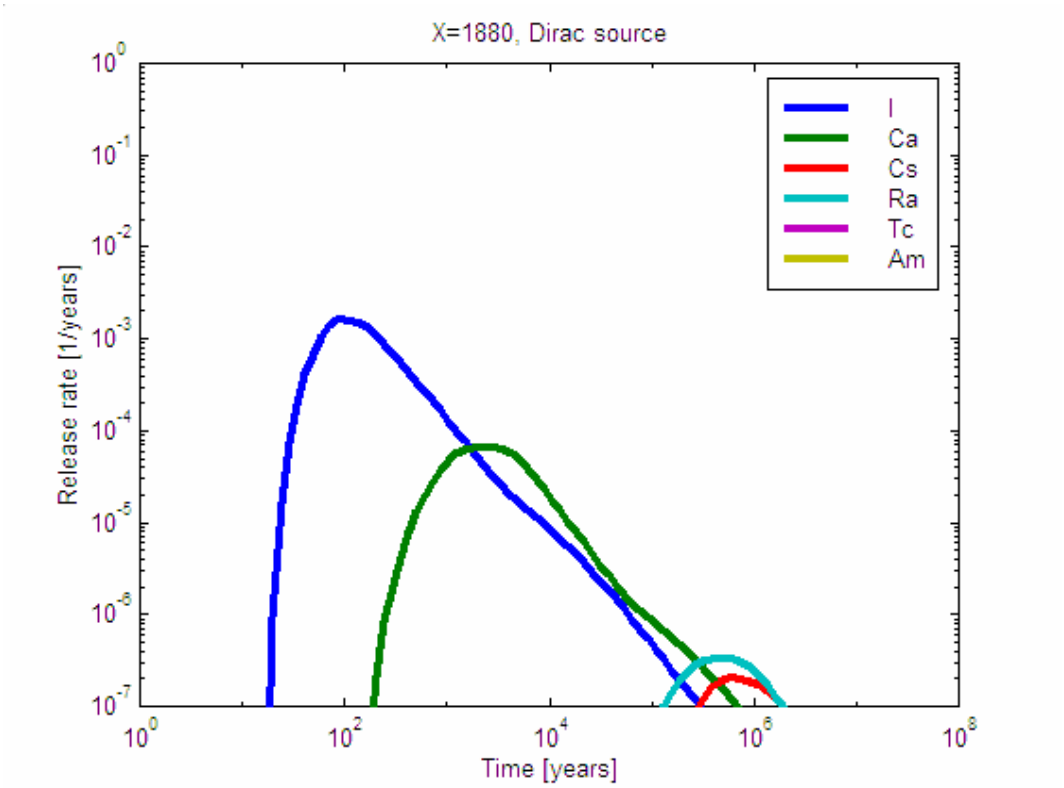

Figure 4-21. *Breakthrough curves at easting=1880 for the Dirac pulse injection source term.*

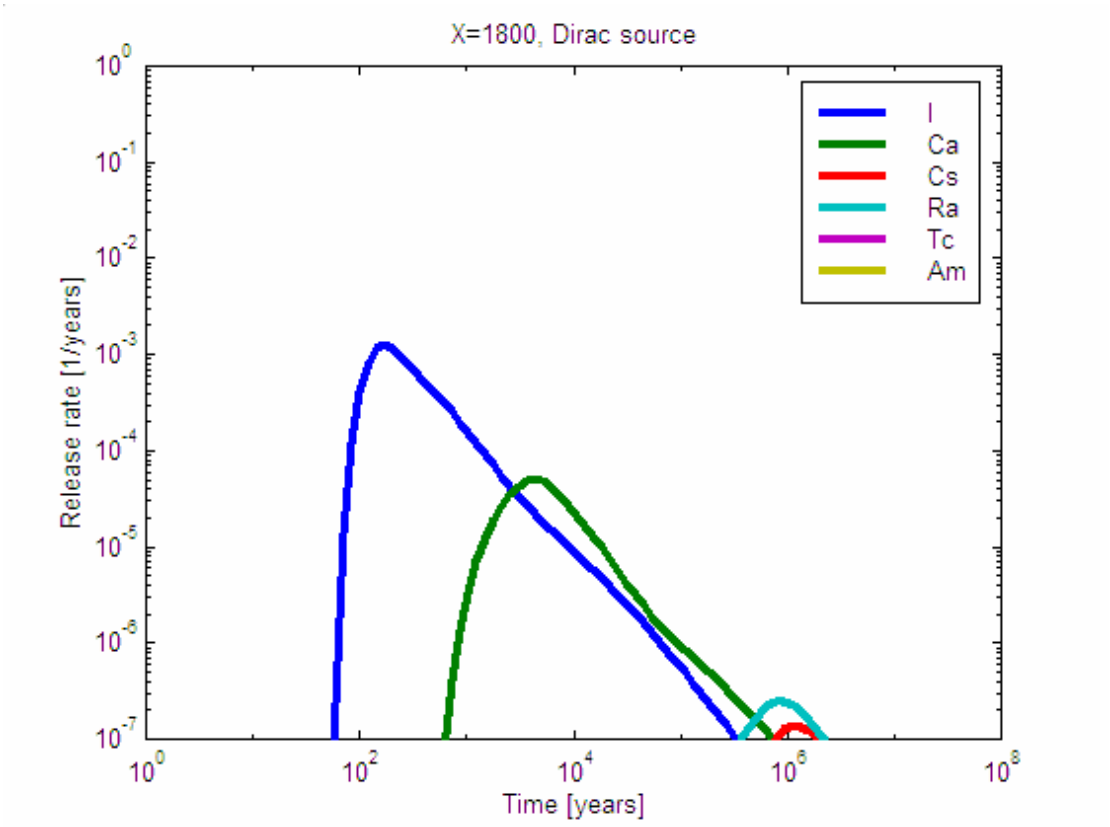

Figure 4-22. *Breakthrough curves at easting=1800 for the Dirac pulse injection source term.*

Breakthrough times for recovery of 5, 50 and 95% of the Dirac pulse injection

Table 4-8. Breakthrough times at the different control planes for the Diracpulse injection function source term.

Easting=1920						
	I	Ca	Cs	Ra	Tc	Am
t_05 [y]	14	247	91 740	53 570	321 900	944 100
t_50 [y]	144	3 039	1 130 000	551 300	5 674 000	16 640 000
t_95 [y]	15 270	460 800	>1E8	48 810 000	>1E8	>1E8
Easting=1880						
	I	Ca	Cs	Ra	Tc	Am
t_05 [y]	70	1 483	460 800	321 900	2 314 000	6 788 000
t_50 [y]	866	15 270	6 788 000	3 313 000	34 100 000	>1E8
t_95 [y]	385 100	4 742 000	>1E8	>1E8	>1E8	>1E8
Easting=1800						
	I	Ca	Cs	Ra	Tc	Am
t_05 [y]	144	3 039	944 100	551 300	4 742 000	13 910 000
t_50 [y]	1 240	21 850	11 630 000	4 742 000	58 390 000	>1E8
t_95 [y]	551 300	9 717 000	>1E8	>1E8	>1E8	>1E8

Maximum release rate

The maximum release rates follow the general behaviour observed already in the assessment of the F-factor. This means that the major retention takes place at the beginning of the flow paths. Especially, results for the Dirac pulse injection source shows that there is only minor change in the peak levels of the breakthrough curves between the second and third control planes, but major change between first and second control planes.

The second control plane is located about 1/3 distance of the third control plane (outer boundary of the model) from the source. Still, majority of the retention takes place in this very first part of the flow path. This also supports the interpretation made earlier that flow paths tend to accumulate to the larger structures that provide much less retention than the smaller ones.

Maximum release rate using extended injection

Table 4-9. Maximum release rates at the different control planes for the 1000 years injection of 1 MBq/yr.

Maximum release rate [Bq/yr]						
	I	Ca	Cs	Ra	Tc	Am
Easting=1920	7.67E+05	3.12E+05	1.58E+03	1.99E+03	2.38E+02	8.11E+01
Easting=1880	5.14E+05	6.60E+04	2.05E+02	3.27E+02	3.11E+01	1.13E+01
Easting=1800	4.48E+05	4.91E+04	1.39E+02	2.46E+02	2.11E+01	7.79E+00

Maximum release rates using Dirac pulse injection

Table 4-10. Maximum release rates at different control planes for the Dirac pulse injection source term.

Maximum release rate [Bq/yr]						
	I	**Ca**	**Cs**	**Ra**	**Tc**	**Am**
Easting=1920	1.38E-02	4.00E-04	1.58E-06	1.99E-06	2.38E-07	8.11E-08
Easting=1880	1.63E-03	6.62E-05	2.05E-07	3.27E-07	3.11E-08	1.13E-08
Easting=1800	1.26E-03	5.00E-05	1.39E-07	2.46E-07	2.11E-08	7.79E-09

4.3 Task 6F

4.3.1 Flow

Description of flow paths

Flow field of the Task 6F is exactly defined in the task definition (see Section 2.5). All information needed for the transport calculations is given in the task definition. In this case the flow paths can be envisaged, for example, as 20 m long straight lines connecting the source line and the control line.

Water residence time distribution

Water residence time distribution is also defined in the task definition. There are three different cases that give water residence times of 0.1 years, 1 year and 10 years. Modelling of the Task 6F uses directly water residence times given in the task definition.

4.3.2 Transport

F-factor – ratio flow wetted surface to water flow

F-factor is represented by the equivalent parameter β, which has been applied in the modelling. F-factors for the different modelling cases of the Task 6F are readily calculated from the task definition. It is assumed that the fracture apertures given in the task definition can be used as effective transport apertures. The complexity factors of the fractures are not taken into account. The F-factor (or β) can then be calculated through the definition $\beta = t_w / b$, where b is the half (transport) aperture and t_w is the groundwater residence time.

Table 4-11. F-factor (β) in the different calculation cases of the Task 6F. The names of the calculation cases are shown in parenthesis after the β-values.

	Groundwater transit time		
Structure type	**0.1 [yr]**	**1 [yr]**	**10 [yr]**
β [yr/m], Type 1	776 (A1)	7 760 (B1)	77 600 (C1)
β [yr/m], Type 2	996 (A2)	9 960 (B2)	99 600 (C2)

Breakthrough time history for the tracers

Transport simulations of the Task 6F are performed only for the Dirac pulse injection source term. Figures 4-23 to 4-25 show the simulated breakthrough curves.

It can be noted that the heterogeneity in the matrix properties, i.e. the layered structure of the immobile zones, does not affect the maximum release rates (Table 4-13). However, the additional highly porous immobile zones in the Type 1 fractures provide additional delay to the breakthrough curves compared with the Type 2 fracture breakthrough curves (see also Table 4-12).

Behaviour of the system when the flow rates are changed is as expected. In the low flow rates (Case C) the difference between Type 1 and Type 2 fracture breakthrough curves diminishes, because most of the immobile zones get saturated by the tracers. In the Case C large portion of the retention is caused by the altered zone and rock matrix. In this cases the additional delay in the breakthrough curves provided by the small volumes of high porosity materials is not to very significant.

The series of calculation cases using different flow rates exemplifies quite clearly the problems that are faced by the in-situ tracer tests and their application to the PA. The role of the small scale heterogeneity to the average matrix retention properties is different in the PA than it is in the in-situ experiments. Case A shows that prediction of the breakthrough time in the in-situ flow field depends almost solely on the accuracy of the microstructural model along the flow path. In the PA flow conditions the retention properties are averaged over much larger volumes of the rock matrix making it easier to provide accurate estimates of the average matrix properties.

Breakthrough curves for the Dirac pulse injection

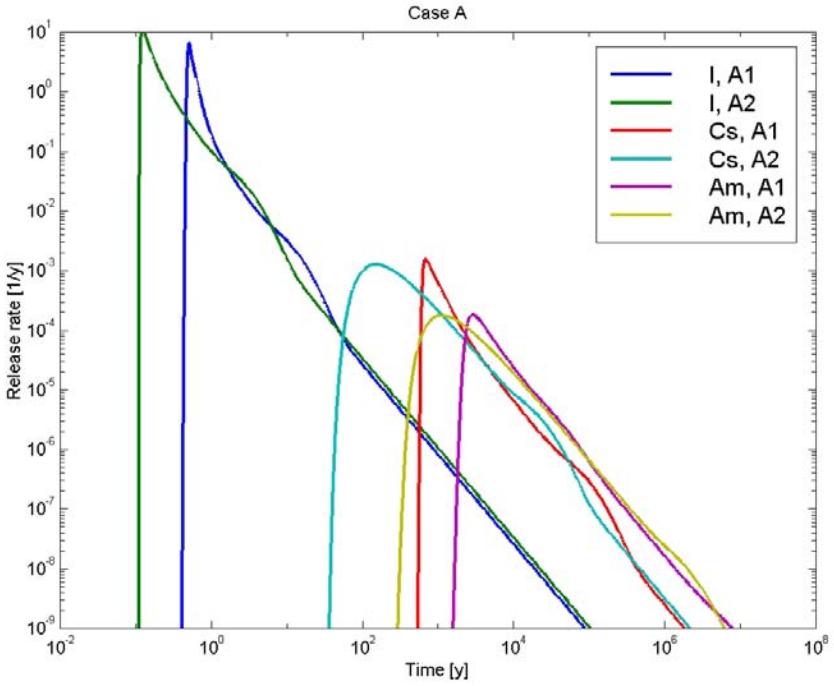

Figure 4-23. *Simulated breakthrough curves of the calculation Case A, groundwater residence time 0.1 years. Case A1 indicates transport through the Type 1 fracture and Case A2 indicates transport through the Type 2 fracture.*

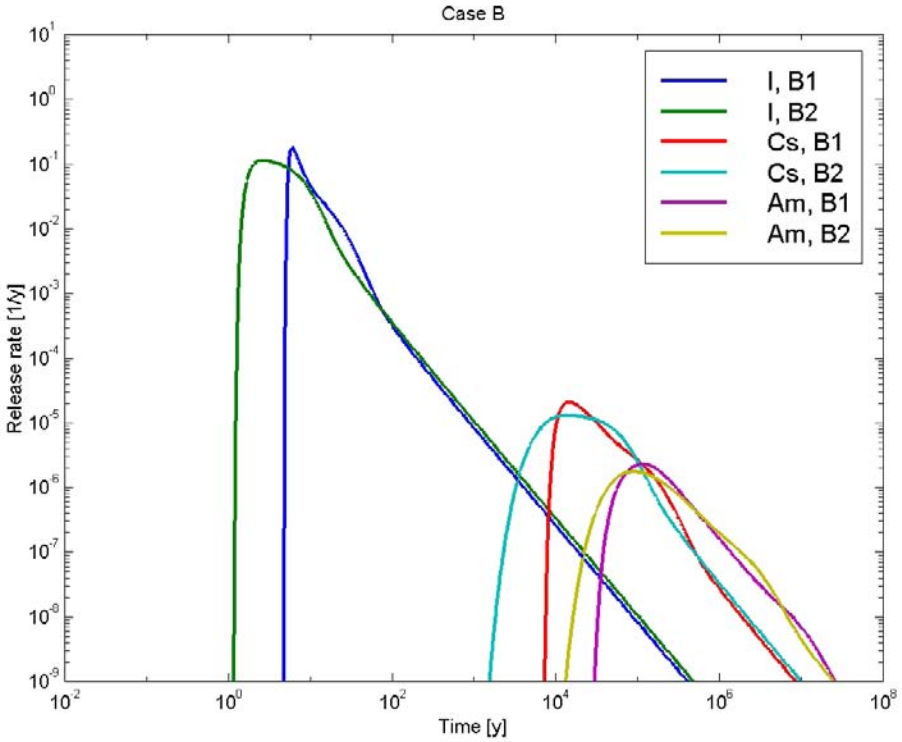

Figure 4-24. *Simulated breakthrough curves of the calculation Case B, groundwater residence time 1 year. Case B1 indicates transport through the Type 1 fracture and Case B2 indicates transport through the Type 2 fracture.*

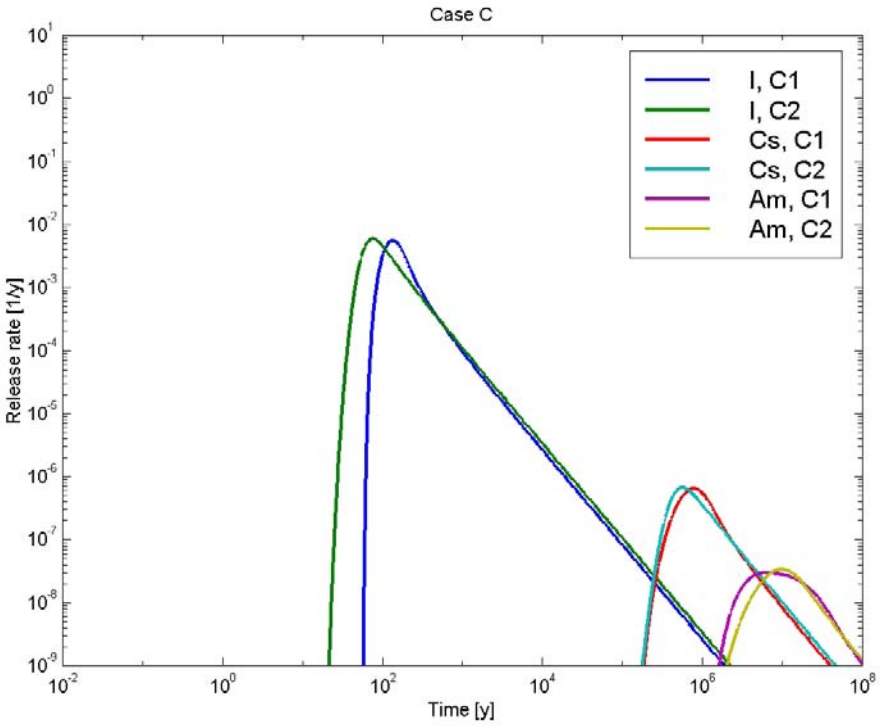

Figure 4-25. *Simulated breakthrough curves of the calculation Case C, groundwater residence time 10 years. Case C1 indicates transport through the Type 1 fracture and Case C2 indicates transport through the Type 2 fracture.*

Breakthrough times for mass recovery of 5%, 50% and 95% in the Dirac pulse injection

Table 4-12. Simulated breakthrough times for recovery of 5%, 50% and 95% of the injected mass for different tracers and different calculation cases.

		t_05 [yr]	t_50 [yr]	t_95 [yr]
Case A1	**I-129**	4.9E-01	5.9E-01	6.5E+00
	Cs-137	6.6E+02	1.2E+03	5.2E+04
	Am-241	2.6E+03	7.4E+03	3.9E+05
Case A2	**I-129**	1.2E-01	2.0E-01	4.6E+00
	Cs-137	1.2E+02	8.3E+02	3.7E+04
	Am-241	9.2E+02	6.0E+03	6.6E+05
Case B1	**I-129**	5.7E+00	1.0E+01	1.2E+02
	Cs-137	1.3E+04	5.5E+04	1.0E+06
	Am-241	8.3E+04	4.1E+05	1.8E+07
Case B2	**I-129**	2.2E+00	6.9E+00	1.8E+02
	Cs-137	9.8E+03	5.1E+04	1.7E+06
	Am-241	7.1E+04	5.8E+05	2.3E+07
Case C1	**I-129**	1.0E+02	2.1E+02	1.1E+04
	Cs-137	5.2E+05	1.4E+06	8.7E+07
	Am-241	4.7E+06	2.4E+07	>1E8
Case C2	**I-129**	6.2E+01	1.9E+02	1.6E+04
	Cs-137	4.5E+05	1.6E+06	>1E8
	Am-241	6.1E+06	2.5E+07	>1E8

Maximum release rates using Dirac pulse injection

Table 4-13. Maximum release rates for the different calculations cases and tracers.

	I-129	Cs-137	Am-241
A1	6.71E+00	1.55E-03	1.82E-04
A2	1.11E+01	1.26E-03	1.75E-04
B1	1.78E-01	2.07E-05	2.27E-06
B2	1.14E-01	1.28E-05	1.75E-06
C1	5.56E-03	6.48E-07	2.97E-08
C2	5.94E-03	6.69E-07	3.38E-08

4.4 Task 6F2

4.4.1 Flow

Description of flow paths

The flow field of the Task 6F2 is very simple. It is completely defined by a few parameters as in the case of the Task 6F. The flow system concentrates only on the retention, i.e. advective delay through the system is not taken into account at all.

For the Task 6F2 purposes flow paths are completely defined by the F-factors (or β) of the transport paths.

Water residence time distribution

There is no water residence time distribution for Task 6F2, because all simulations are made only for the tracer retention.

4.4.2 Transport

F-factor – ratio of flow wetted surface to water flow

The flow system is composed of two parallel fractures. A total F-factor is defined for the whole system and it is kept fixed for all simulations. The total F-factor is then divided between the Type 1 and Type 2 fractures using following divisions of the total flow rate between the two fractures: all to one fracture, 8:1, 4:1, 2:1 and 1:1. Table 4-14 collects the data used in the different calculation cases and the corresponding F-factors of the flow paths through the fractures.

Table 4-14. Definition of the β for the two fracture system in different calculation cases of Task 6F2. β_1 means F-factor to the Type 1 fracture and β_2 to the Type 2 fracture.

Case	β_1 [yr/m]	β_2 [yr/m]	Transport channel: width 0.1 m and length 20 m		Total flow rate
			Q1 [litre/yr]	Q2 [litre/yr]	Q_{tot} [litre/yr]
1	7 752	7 752	0.52	0.52	1.03
2	5 814	11 628	0.69	0.34	1.03
3	4 845	19 380	0.83	0.21	1.03
4	4 360	34 884	0.92	0.11	1.03
5	3 876		1.03		1.03
6	11 628	5 814	0.34	0.69	1.03
7	19 380	4 845	0.21	0.83	1.03
8	34 884	4 360	0.11	0.92	1.03
9		3 876		1.03	1.03

Breakthrough time history for the tracers

Breakthrough curves are calculated for three different tracers: I-129, Cs-137 and Am-241. Calculations are made only for the retention due to the matrix diffusion and sorption. Figures 4-26 to 4-28 show the breakthrough curves for all calculations cases without advective delay.

Results indicate that retention and the corresponding attenuation of the tracer discharge peak levels are very sensitive to the flow rate. The assumption of well mixed conditions at the inlet of the two fracture system means that the tracer masses through the path are proportional to the flow rate. However, the inequality of the tracer mass going through the fractures cannot explain the results. Retention and attenuation of the release rates due to the matrix diffusion need to have a very significant affect on the results.

Examination of the I-129 breakthrough curves (Figure 4-26) demonstrates that contribution of the both flow paths can be observed in the breakthrough curves only if the flow rate is almost evenly divided between the two flow paths. Already a factor of two difference in the flow rate means that one of the flow paths dominates. This behaviour seems to be stronger for the sorbing tracers (Figure 4-27 and Figure 4-28). The reason for this is that the retention is stronger for the sorbing tracers and therefore the influence fracture type to the breakthrough curve is smaller, i.e. additional delay provided by the small but porous immobile zones is small compared to the overall retardation.

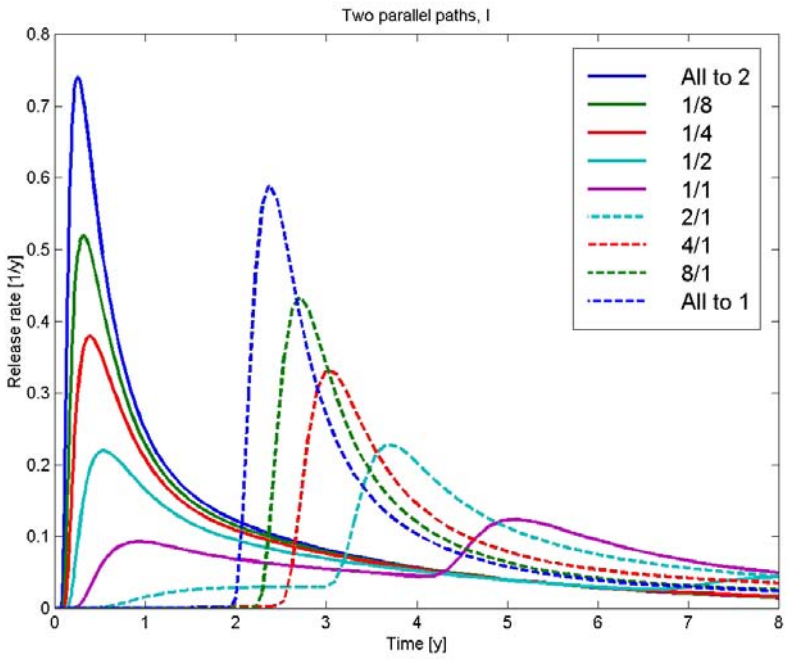

Figure 4-26. *Breakthrough curves for the I-129 through the system of two parallel fractures. Numbers in the legend indicate division of the total flow rate between the Type 1 and Type 2 fracture (Q1/Q2).*

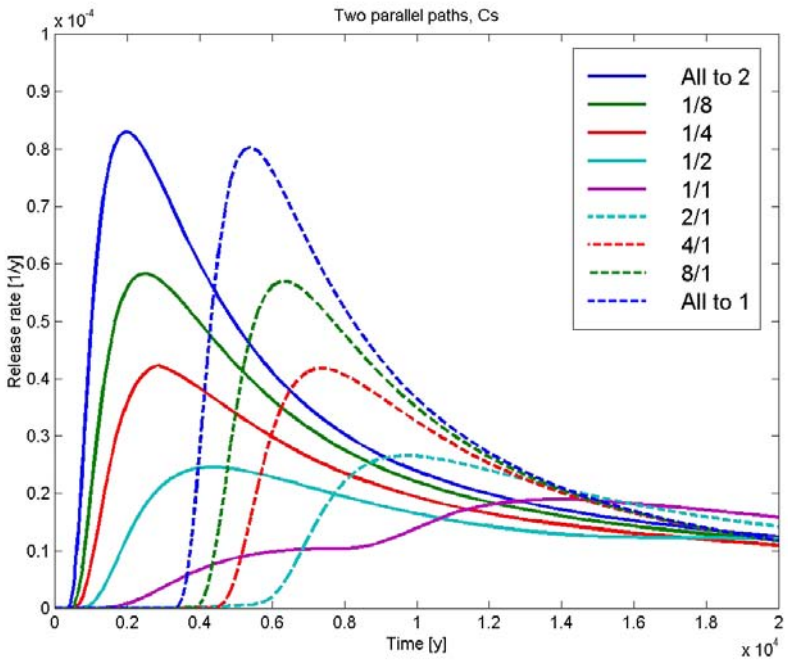

Figure 4-27. *Breakthrough curves for the Cs-137 through the system of two parallel fractures. Numbers in the legend indicate division of the total flow rate between the Type 1 and Type 2 fracture (Q1/Q2).*

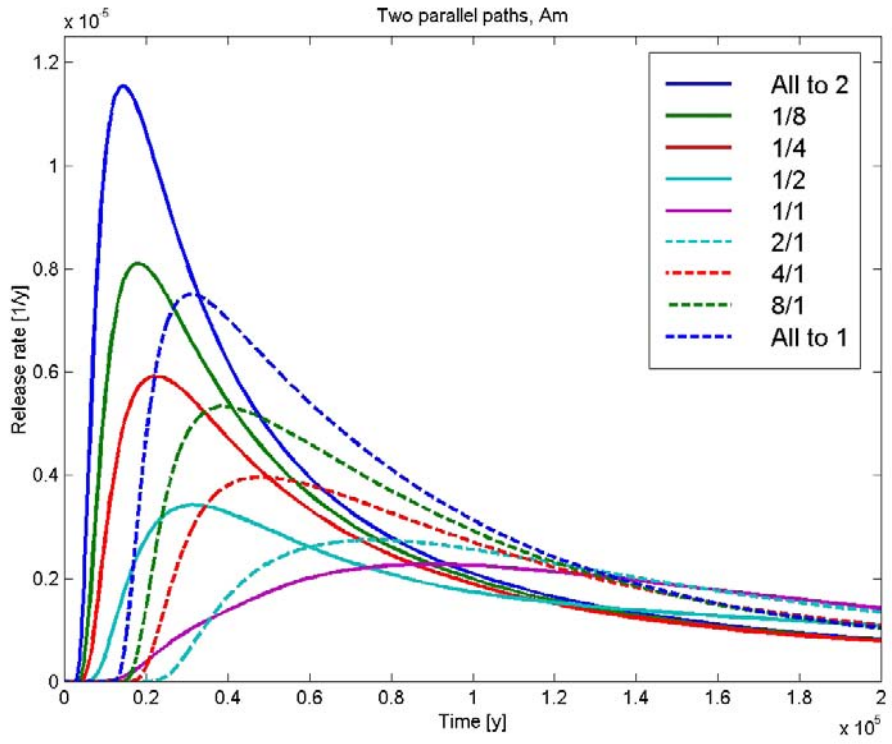

Figure 4-28. *Breakthrough curves for the Am-241 through the system of two parallel fractures. Numbers in the legend indicate division of the total flow rate between the Type 1 and Type 2 fracture (Q1/Q2).*

5 Discussion and conclusions

5.1 Discussion of results

5.1.1 Task 6D

Qualitatively, the behaviour is quite similar for both non-sorbing and sorbing tracer. Comparing the non-sorbing Iodine and the most sorbing tracer Americium indicates that release rates are controlled by the fault gouge, altered and unaltered rock matrix. The similarity between sorbing and non-sorbing tracers is not surprising, because breakthrough curves are followed to almost full recovery and radioactive decay is not taken into account. Sorption in the immobile pore space does not affect the penetration depth visited by the tracer but it does affect the time scale needed to reach the different depths.

Retention seems to take place mainly in the fracture coating of the flow field of the Task 6D. Contributions of the different matrix immobile zones to the breakthrough curves show that about half of the total retention time is caused by the coating (cf. contributions of the individual immobile layers in Figure 5-1). Fault gouge has more important role to the overall retention for the non-sorbing tracers than the sorbing ones and cataclasite has only a minor role in the overall retention.

The role of the fault gouge indicates sensitivity of the expected retention on the geological and structural properties of the fracture wall rock. Especially, for the non-sorbing tracers fault gouge has an important role to the retention, although fault gouge exists only in the Type 1 features. About 1/10 of the total hydrodynamic control of retention (F-factor, β) accumulates in the Type 1 fractures. Subtle increase of the β of the Type 1 features would increase significantly the importance of the fault gouge to the overall retention.

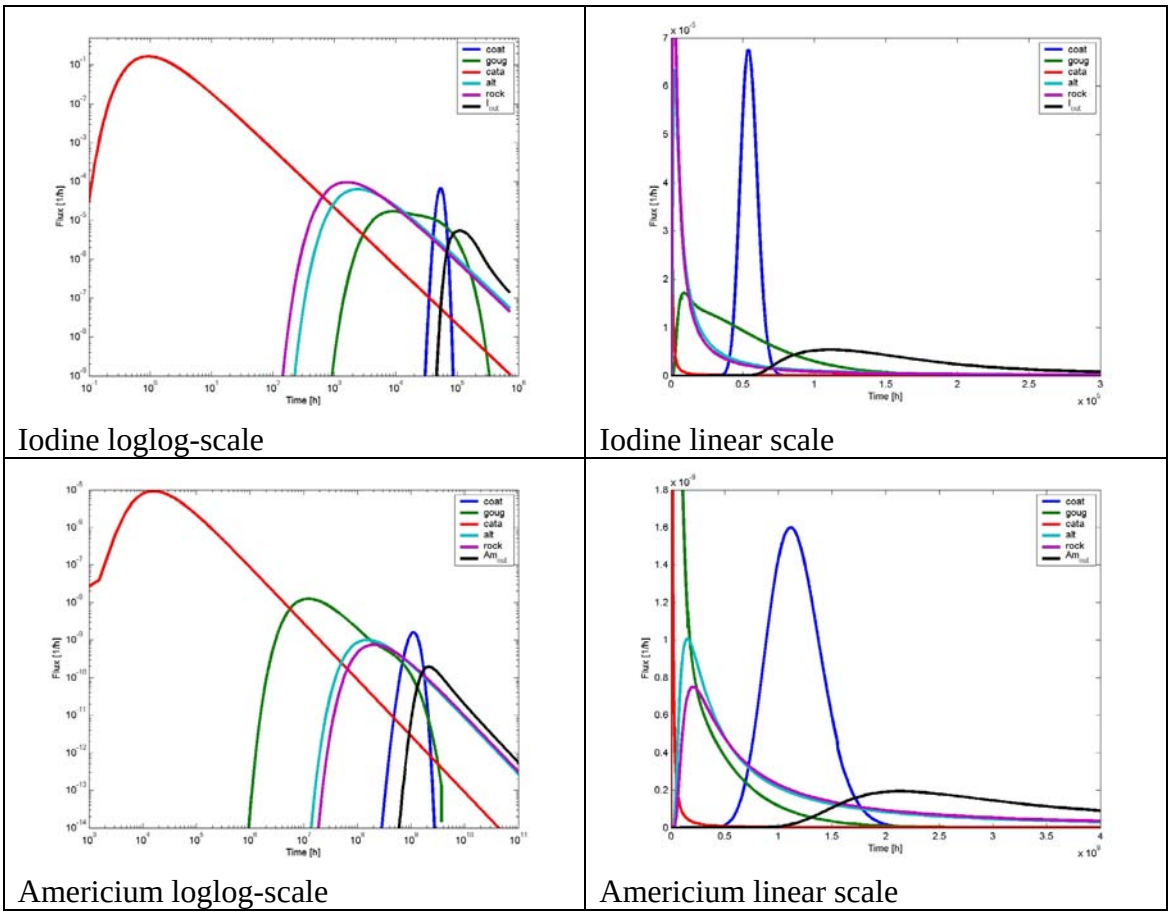

Iodine loglog-scale | Iodine linear scale

Americium loglog-scale | Americium linear scale

Figure 5-1. *Contributions of the individual immobile layers to the breakthrough curves of the Iodine and Americium (retention by sorption and matrix diffusion, without advective delay). Tracer breakthrough curves are shown by black lines.*

5.1.2 Task 6E

Task 6E (PA scale) results are compared with the Task 6D (SC scale) results. This comparison is performed by examining the contributions of the individual immobile zones in both models. As in the case of Task 6D, simulation results are presented for the non-sorbing tracer Iodine and for the most sorbing tracer Americium. Task 6E results are presented for all three different control planes.

Contributions of the individual immobile matrix layers are shown in the Figure 5-2. It is evident from the individual contributions of the immobile layers that in the Task 6E flow field the fracture coating and fault gouge get saturated for all tracers and all control points (their contributions are delta functions). Cataclasite and altered zone show clear indications of the limitation of the thickness of these immobile layers, i.e. tailings of their contributions do not follow the $t^{-3/2}$ power-law. Also, it can be observed that they become more or less fully saturated for the flow paths that extend to the Easting=1800, i.e. path length of 200 to 300 meters.

The level of the maximum release rate is controlled by the intact rock in all cases presented in Figure 5-2. In the case of the Task 6D release rates are also influenced by the limited volume immobile zones like the altered zone.

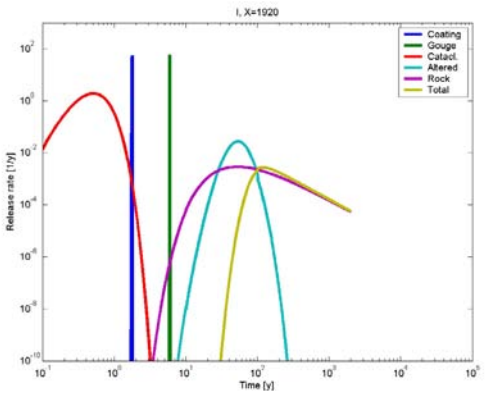

Iodine, Easting=1920

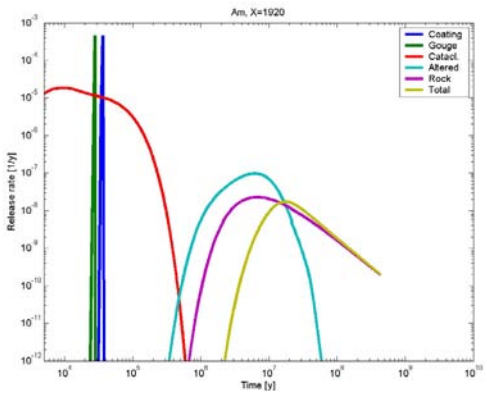

Americium, Easting=1920

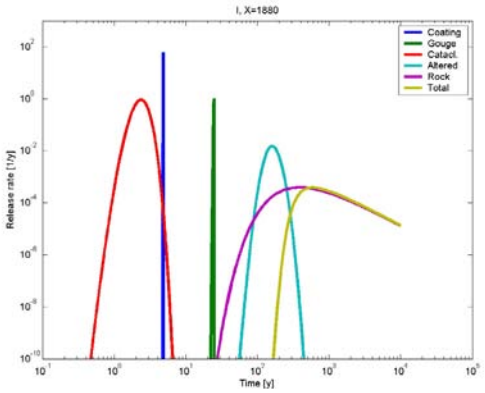

Iodine, Easting=1800

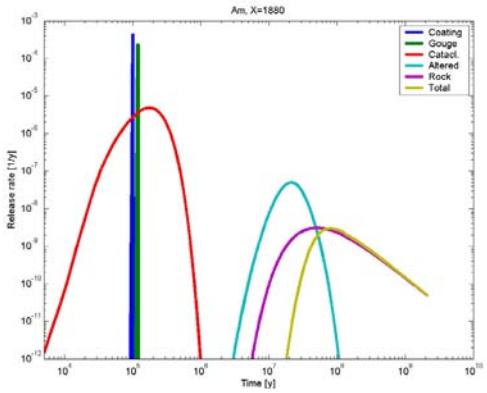

Americium, Easting=1880

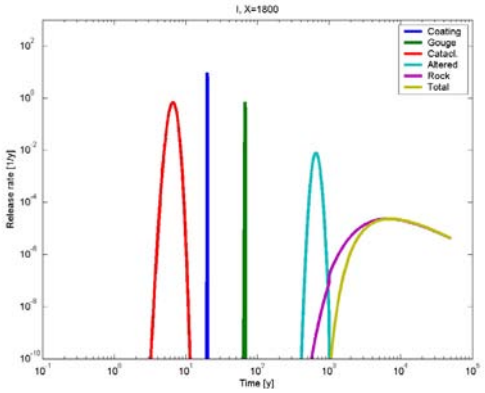

Iodine, Easting=1800

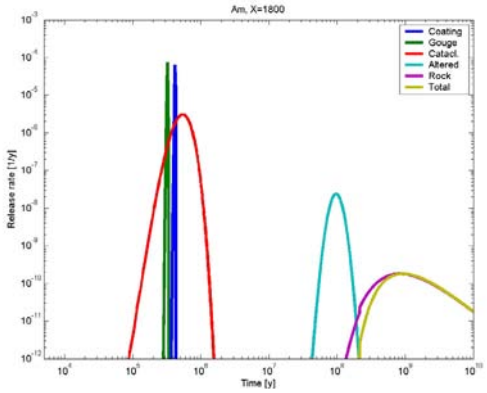

Americium, Easting=1800

Figure 5-2. *Contributions of the individual immobile zones to the breakthrough curves. Tracer breakthrough curves are shown by yellow lines.*

5.1.3 Task 6F

Task 6F concentrates on the retention in the individual fracture types. In this sub-task differences in retention properties arise from the microstructural models of the fracture types.

Contribution of the different geological materials to the overall retention is examined in the same way as in the Task 6D and 6E. Figure 5-3 shows the contribution of the different immobile layers to the overall retention in different fracture types for a non-sorbing tracer.

Following observations can be drawn about the contribution of the limited volume immobile zones to the overall retention:

- For large flow rates and early breakthrough times also the limited volume immobile zones show infinite matrix -type behaviour.
- There is a fixed time when the contribution of the limited volume of the immobile zone deviates from the infinite behaviour (i.e. $t^{-3/2}$ tailing). This time is directly proportional to the diffusion time through the immobile layer ($t_D \sim 1/C \cdot L^2/D_p$), where the factor C is describes the coverage of the immobile zones along the flow path.
- Smaller flow rates cause more retardation of the breakthrough curve; however there is a maximum retention that a limited volume immobile zone can provide. When also the early part of the breakthrough curve is retarded to the time of the maximum retention then the contribution of that immobile zone is just a Dirac pulse, i.e. the layer is saturated.

Based on the conclusion above it is clear that for the smaller flow rates (PA scale) the differences between the fracture types (and different microstructural model) is manifested only by an additional delay caused by the larger volume of the immobile pore space in the complex features. Sorbing tracers behave in the same way as the non-sorbing tracers. However, the time scales are different, depending on the sorption properties.

It should be noted that the situation can be totally different when the radioactive decay is taken into account. The delay caused by the saturated but relatively thin layers can be large compared to the half-life of the nuclide. This would mean that nuclides, which have short half-life but are strongly sorbing, do not penetrate to that deep into the rock matrix as the non-sorbing ones.

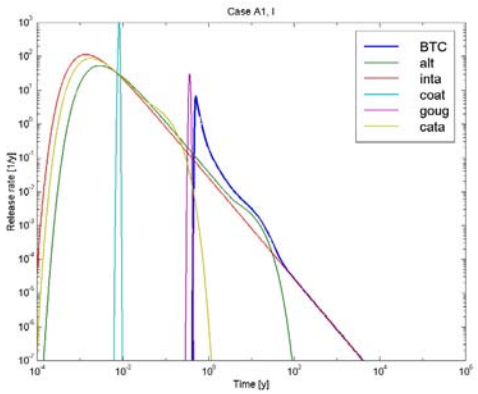

Iodine, Case A1, Fracture Type 1

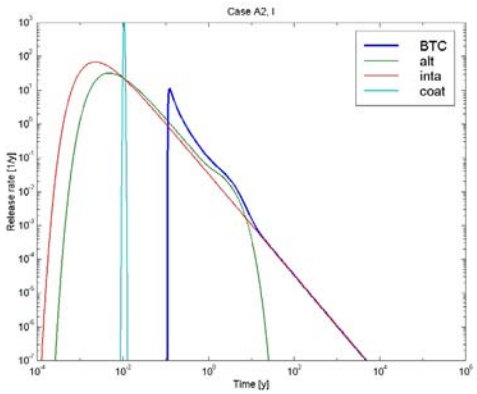

Iodine, Case A2, Fracture Type 2

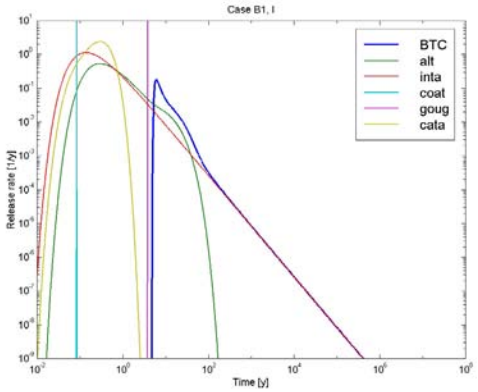

Iodine, Case B1, Fracture Type 1

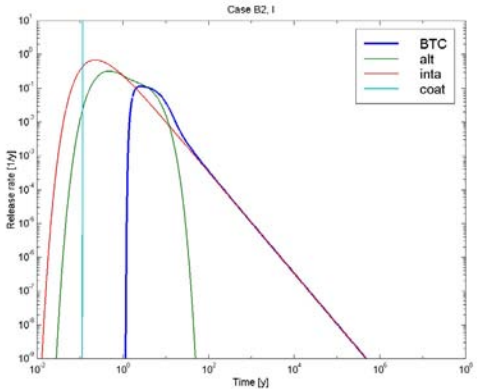

Iodine, Case B2, Fracture Type 2

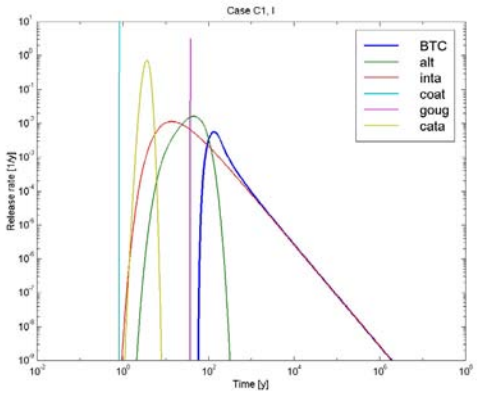

Iodine, Case C1, Fracture Type 1

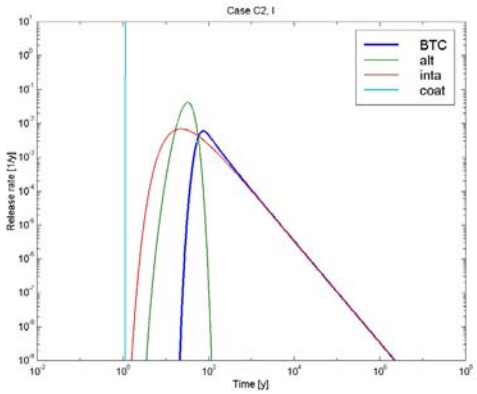

Iodine, Case C2, Fracture Type 2

Figure 5-3 *Contribution of the individual immobile zones to the overall retention for the non-sorbing I-129 in the different Task 6F calculation cases and for the different fracture types.*

5.1.4 Task 6F2

Task 6F2 is a direct extension of the Task 6F. In Task 6F different fracture types are studied separately. Task 6F2 studies a complex structure that is composed of parallel Type 1 and Type 2 fractures. The main emphasis of the Task 6F2 modelling is the coupling between flow field and retention properties.

Results of the Task 6F2 show that the retention caused by the matrix diffusion is very sensitive to the flow rate. Usually, the flow path of the highest flow rate dominates the breakthrough curve. It carries larger mass of the tracer, but more importantly retention and corresponding attenuation of the solute discharge rate is much smaller along the high flow rate path than they are along the flow paths of smaller flow rates. The two fracture system of Task 6F2 modelling shows clear dominance of the higher flow rate path already for a factor two difference in the flow rates.

5.2 Main conclusions

The modelling indicates that retention in the site characterisation scale is easily dominated by geological materials that are small in volume but highly porous, like the fault gouge. Importance of these materials in the performance assessment scale may vary depending on the nuclide due to the varying sorption properties and radioactive decay (decay is not considered in Task 6). It is likely that thin layers of geological materials do not have such an important role in the performance assessment conditions than they have in the site characterisation conditions.

Flow paths of the Task 6E indicate that all other geological materials than the unaltered rock matrix get easily saturated in the performance assessment conditions. In practice, this means that it is probably sufficient to represent the immobile zones in the performance assessment by the unaltered rock matrix only. However, also the immobile zones in the other geological materials need to be known and characterised if the exact time solute discharge is crucial. The immobile zones of limited volume cause equilibrium sorption type of delay to the discharge time that can be important for the short half-life nuclides.

5.3 Lessons learned and implications for Task 6 objectives

The main lesson learned has been that the link between the site characterisation models and performance assessment models need to be evaluated carefully. Some of the geological materials, like fault gouge, provide considerable retention but their volumes are also significantly limited.

Regarding the objectives of Task 6 (Benabderrahmane at al., 2000) following conclusion can be drawn from the present modelling:

Objective 1: Assess simplifications used in PA models.

The microstructural model of the PA models is usually much simpler than the SC model. It seems that a rather simple microstructural model will do in the PA, but the average retention properties cannot be determined from the SC tracer tests. On the other hand, process understanding of the key retention processes in the PA models can be demonstrated in the SC scale. SC modelling requires detailed information on the microstructural model and flow.

Objective 2: Assess the constraining power of tracer (and flow) experiments for PA models.

SC tracer tests are not able to directly provide transport parameters for the PA. The reason is that in the SC scale the matrix properties are averaged over a thin layer next to the fracture. In many cases this layer has significantly different properties compared to the much larger scale of averaging in the PA flow conditions.

Objective 3: Provide input for site characterisation programs from a PA perspective

Demonstration of the process understanding needs to be performed in the SC scale. However, control of the flow conditions in-situ, identification of the active flow paths and the corresponding fracture types and immobile zones is very challenging.

Objective 4: Understand the site-specific flow and transport behaviour at different scales using SC models.

Task 6 provides understanding about the connection between the retention, variable flow conditions and multiple immobile zones (cf. objectives 1-3).

6 References

Benabderrahmane, H., Dershowitz, W., Selroos, J.-O., Uchida, M. and A. Winberg, 2000. Task 6: Performance Assessment Modelling Using Site Characterisation Data (PASC), November 28, 2000.

Dershowitz, W., Winberg, A., Hermanson, J., Byegård, J., Tullborg, E.-L., Andersson, P., and M. Mazurek, 2003. TASK 6C, A Semi-Synthetic Model of Block Scale Conductive Structures at the Äspö Hard Rock Laboratory, SKB International Progress Report IPR-03-13.

Elert, M. and J.-O. Selroos, 2002. TASK 6D Modelling task specification, Version 1.0. Memorandum, November 2002.

Elert, M. and J.-O. Selroos, 2004a. TASK 6E Modelling task specification, Version 3.0. Memorandum, January 2004.

Elert, M. and J.-O. Selroos, 2004b. TASK 6F Sensitivity analysis. Modelling task specification, Simplified "Test Bench" transport calculations, Version 3.0, Memorandum, December 2004.

Elert, M. and J.-O. Selroos, 2004c. TASK 6F2 Sensitivity analysis. Modelling task specification. Additional tasks, Version 1.0. Memorandum, December 2004.

Andersson, P, Byegård, J. and A. Winberg, 2002. Final report of the TRUE Block Scale Project, 2. Tracer tests in the block scale. May 2002. SKB Technical Report TR-02-14.

FEFTRA, 2004. The finite element program package for modelling of groundwater flow, solute transport and heat transfer, VTT Processes. http://www.vtt.fi/pro/pro1/feftra

Cvetkovic, V. and R. Haggerty. Transport with multiple-rate exchange in disordered media. May 2002, Phys. Rev. E, Vol. 65, 051308.

Poteri, A., 2002. Modelling of the Task 6A, 6B and 6B2 using Posiva streamtube approach. SKB, International Progress Report, IPR-04-41.